Journal Pre-proof

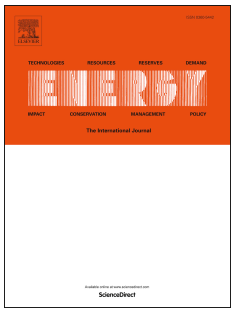

Numerical investigation of a novel tower solar chimney concept

Hakim KEBABSA, Mohand Said LOUNICI, Ahmed DAIMALLAH

PII: S0360-5442(20)32155-1

DOI: https://doi.org/10.1016/j.energy.2020.119048

Reference: EGY 119048

To appear in: *Energy*

Received Date: 3 April 2020

Revised Date: 25 July 2020

Accepted Date: 8 October 2020

Please cite this article as: KEBABSA H, Said LOUNICI M, DAIMALLAH A, Numerical investigation of a novel tower solar chimney concept *Energy*, https://doi.org/10.1016/j.energy.2020.119048.

Numerical investigation of a novel tower solar chimney concept

Hakim KEBABSA [a], Mohand Said LOUNICI [a*],
Ahmed DAIMALLAH [a]

[a] LEMI, Université M'hamed Bougara, Boumerdes, 35000, Algeria.

Corresponding author: mslounici@univ-boumerdes.dz, mslounici@hotmail.com, phone: +213697688074, Fax: +21324912951

Abstract

Divergent tower solar chimney power plant is an attractive upgrading of the solar chimney system. However, boundary layer separation (BLS) phenomenon can appear when the divergence angle exceeds a specific value, inducing system performance degradation. The present paper proposes a novel solar chimney tower concept, named annular tower solar chimney power plant (ATSCPP), to deal with BLS phenomenon and improve the divergent tower system. Accordingly, the influence of exterior tower radius (ETR) and interior tower radius (ITR) were evaluated, using the Spanish prototype. Simulations were carried out using a 3D model. The results indicate that flow behavior, power output and thermal efficiency shows a strong sensitivity to the change of both ETR and ITR. The best case is obtained when (ETR=17m, ITR=13m). The new solar chimney tower concept allowed a significant increase in the driving potential. The total improvement in power output reaches 32%. An improved concept which allows a compromise between induced cost and performance gain of the system is also proposed.

Keywords: Solar chimney; divergent tower; annular tower; natural convection; solar energy.

Introduction

During several decades, the world has continued to rely on fossil energy resources, namely oil, gas, and cheaper resources such as coal. Consequently, air pollution and the acceleration of climate change become a serious problem. The need for other solutions for energy supply is crucial to avoid global environmental catastrophes.

The rapid growth in energy systems and the vital role that alternative energies play in the energy mix encourage the transition to alternative sources. The focus on renewable energy continues to increase for reasons, especially related to environmental concern. As a result, in china only, renewables influence energy-related emissions falling by 20% as a result of decreasing coal use in power generation [1]. Alternatives offer more benefits than fossil fuel-based generation systems and could satisfy global energy security thanks to the acceleration in the development of these technologies. Consequently, in the five recent years, the renewable cost is considerably coming down. If it continues to decline, building a wind plant will cost-competitive as fuel cost of a conventional plant [1]. In the past few decades and as a result of the transition to renewables, the contribution of fossil energy is reduced in favor of renewable penetration in the energy mix. The renewables double its contribution to electricity generation, i.e., from 18% in 2005, renewables will supply 27% of global energy demand by 2020 and 50% by 2050 [2].

However, there is a wide range of concerns if we intend to generalize the implementation of the renewables, including the problems of storage and setting the infrastructures, especially in third-world countries. Although many regions of the third world have abundant low or zero-carbon sources (solar, wind, and hydro), the unequal distribution of resources, high technology costs, and intermittency remain problems for renewables integration. In these areas, the SCPP, an interesting and simple system of using solar energy

in clean power generation, allows taking the advantages of low-cost effectiveness and zero-carbon-emissions.

Research on SCPP began several decades ago, the first large scale prototype of SCPP was built in Spain. Since then, many studies have focused on optimizing the performance of this type of sustainable generation energy system through numerical, theoretical, and other experimental works. Several methods and theories have been proposed to study the SCPP performances, some focusing on collector and tower, others on the turbo-generator system [3-5].

A series of recent studies such as that conducted by [6-18] has focused on the performances of SCPP collector. In an investigation into optimization of the design of SCPP, Belkhode et al. [8] found from experiments that the Plain glass as a collector material performs better energy rays transmission than the Acrylic sheet, Polycarbonate sheet, and Crystalline sheets. Hussain et al. [9] proposed a hybrid system that integrated the solar chimney with an external heat source through the installation of flue-gas channels in the collector to supply the system with air. As a result, the mass flow rate and collector efficiency enhanced by 12.0%, and 64.0%, respectively. In studies carried out by [10, 11], It is demonstrated that a thermal energy storage system was beneficial since it enhanced the SCPP operating period. Preliminary work on a new SCPP system structure with a perforated absorber layer in the middle between both of collector roof and the traditional absorber was undertaken by Li et al. [14]. Li et al. [14] demonstrated that dividing the airflow into two channels led to increase heat transfer surface and perform better heat transfer due to its porosity characteristics and allow more stable power generation. Kebabsa et al. [17] reported a new and more convenient design of a partial-inclined SCPP collector. It is found that airflow was enhanced significantly. It is shown that the optimal configuration (a sloping distance of 0.8 and slope of 9.1) generated higher available power by 16.36% than that of a

conventional system. Li et al. [18] evaluated the performance of a solar chimney power plant (SCPP) by using a comprehensive theoretical model. There was a limitation on the maximum collector radius exists for the maximum attainable power of the SCPP; whereas, no such limitation exists for chimney height in terms of contemporary construction technology.

There have also been numerous studies to investigate turbine design in the SCPP [19-26]. The estimation of the optimized design of wind turbine blades for a solar updraft tower was first carried out by Balijepalli et al. [19]. Results showed that when air velocity is higher (10 m/s), the power output could reach 0.06W for optimized values of blade pitch angle, relative wind angle, and lift force equal to 18.4°, 26.4°, 0.0052 N respectively. One study by von Backstrom et al. [20] examined a typical layout of a solar chimney power plant that has a single axial turbine with radial inflow through inlet guide vanes at the base of the chimney. Results found that turbine efficiency depended on the turbine blade row and turbine diffuser loss coefficients. A recent study by Fluri et al. [21] involved a comparison between the single rotor and counter-rotating turbine layouts using analytical and optimization methods to find the best design parameters. Results found that introducing a limit to the degree of reaction of the turbine to avoid diffusion at the hub had a significant impact on the performance prediction. The study carried out by Fluri et al. [22] Compared between the single vertical axis, the multiple vertical axes, and the multiple horizontal axis turbine configurations. Results showed that the single vertical axis turbine was more advantageous with regards to efficiency. Another study carried by Denantes et al. [23] compared between two counter-rotating turbines, with or without inlet guide vanes to a single-runner system. It is shown that the counter-rotating turbines without guide vanes were more advantageous. It has been argued that the turbine pressure drop factor was in the range of 0.8–0.9 [24-26].

Seminal contributions have been made by studying the performance of SC tower. Zhou et al. [27] investigated the maximum tower height allowing positive buoyancy at the tower

outlet using a theoretical model. Sensitivity analysis was also performed to investigate the effect of various geometrical and atmospheric conditions on maximum tower height. The results showed that the optimal height of 615 m yielded a power output of 102.2 kW. A small scale study by Shirvan et al. [28] was carried out to obtain the potential maximum power output of the SCPP prototype. It is found that the power output enhances with increasing both the chimney diameter and height. Studies such as that conducted by [29-31] have shown that full or partial diverging tower is more beneficial than the conventional tower. In another major study, Koonsrisuk et al. [31] found that the divergent-top tower increased SC's power output.

However, one of the problems met with diverging SC is boundary layer separation and the generation of backflows, especially when the tower's divergence angle exceeds an optimum value for which the driving potential reaches its maximum [31,32]. Several studies [33,34] have found that the eddies generation is responsible for output degradation. In an interesting recent study, the maximum power of 231.7 kW was reached for an optimal divergence angle, which is 11.9 times as high as that for conventional chimney [34]. More characteristics on the different SCPP tower geometries and the optimal configuration were recapitulated in Table 1.

Table 1

Optimum configuration of different diverging SCPP tower.

Article	Tower height (m)	controlling parameter	Optimum case
Xu et al. (2018)	194.6	Divergence angle=0-3-6.04-6.65-7.56-9.08-12.10	Divergence angle=6.04°
Hu et al. (2017)	95	Area ratio=1-2-4-6-8-10-12-14	Area ratio=6
Okada et al. (2015)	0.4	Divergence angle=4	-
Patel et al. (2014)	10	Divergence angle=0-1-2-3	Divergence angle=2°
Koonsrisuk et al.	100	Area ratio=0.25-0.5-0.75-1-2-4-8-16-32	Area ratio=16

(2013)			
Ming et al. (2011)	800	Area ratio= 0.5-0.75-1-1.25-1.5	Area ratio=1.5

Only a few studies have shown the effect of the diverging tower on SCPP performance. Moreover, there is no previous research treating the problem of boundary layer separation when the diverging angle exceeds the optimum, as mentioned earlier. Also, as far as we know, no previous study has investigated the airflow pattern characteristics when the turbine is taken into consideration, which misled the comprehension of the real effect of the diverging tower on SCPP performance and induced imprecise results. Some questions regarding the diverging tower effects remain to be addressed. Taking advantage of diverging tower concept and aiming its improvement, by dealing with boundary layer separation, the present study consists of an investigation of an annular tower as a new concept that would overcome eddies creation in the conventional system. This concept aims to enhance farther diverging tower SCPP performance. Besides, simulations taking into consideration the turbine are conducted.

2. Methodology

Different simulations are carried out using ANSYS FLUENT 16.0. In the following section, a detailed description of the methods adopted and geometric configurations examined is presented.

2.1. Geometrical configurations

The base case adopted in the present study is the Spanish prototype presented by Schlaich et al. [35] and Haaf et al. [36, 37]. The geometric dimensions of this plant are appropriate to show how the annular tower SC can improve the performance of this type of renewable energy generation technology. Hence, all simulation cases take the Spanish prototype [35] as a reference. The main geometric parameters are presented in Table 2.

Table 2

Principal geometric parameters of the Spanish prototype.

Geometric parameter	Dimension (m)
Collector radius (R_c)	122m
Collector inlet height (H_{ci})	1.85m
Collector outlet height (H_{co})	1.85m
Tower height (H_t)	194.6m
Tower radius (R_t)	5.08m
Wind turbine height (H_{wt})	9m

The solution domain was modeled with a 3D calculation. The computational geometry has two symmetry surfaces. So, instead of simulating the full 3D geometry, one quarter (¼) of the system is sufficient to reduce the computational effort. The schematic diagram of the geometry is shown in Fig. 1.

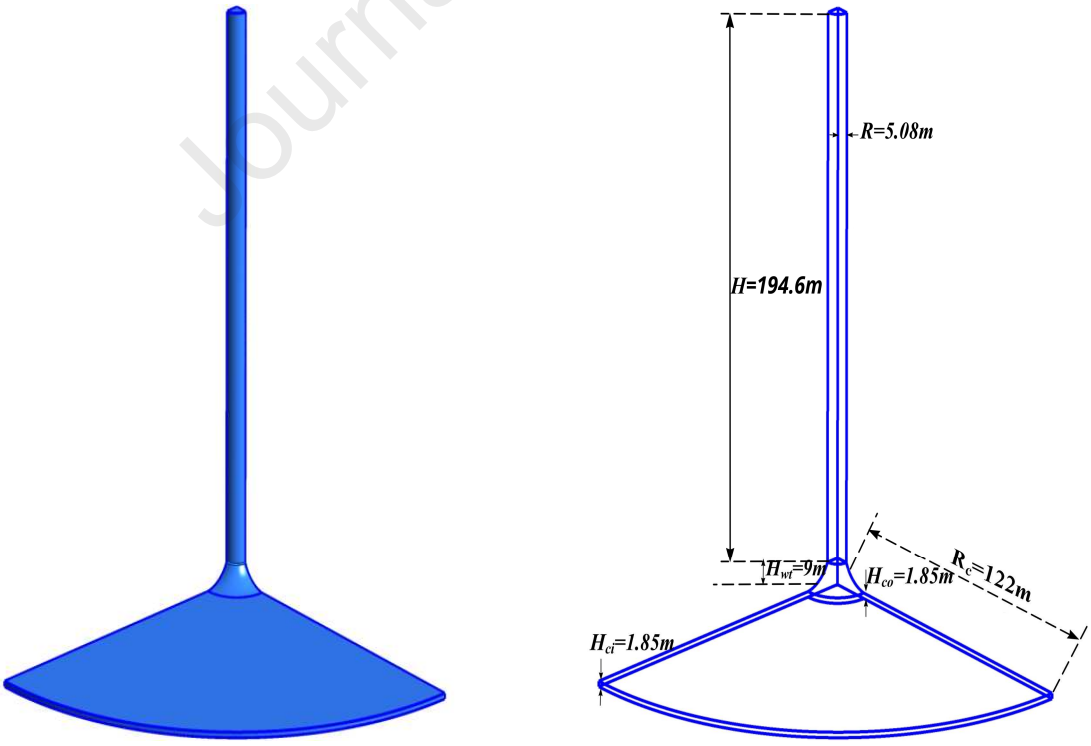

Fig.1. 3D geometry of the Spanish SC.

In the cylindrical chimney, the velocity at the tower inlet is equal to that at the tower outlet, and thus the static pressure recovery is equal to 0. However, for DTSCPP, the inlet velocity is larger than the outlet velocity as simultaneously obtained from the continuity equation (Eq. (6)) and shown in Fig. 7, thus causing positive static pressure recovery. The driving potential is, therefore, increased. It is concluded that besides the same function of producing buoyancy as in a conventional chimney, the divergent tower effectively converts some of the dynamic pressure to static pressure. This leads to variable inlet velocity determined by the surface of the tower outlet. For large enough divergence angle, eddies generation occur, and the effective flow area of the up current is reduced. This will lead to a decrease in static pressure recovery. In many research works [33,34], it is found that eddies generation is responsible for output degradation of the DTSCPP when the divergence angle exceeds an optimum value. However, the ATSCPP allows decreasing the size of the recirculation zone keeping the surface of the outlet more important. The ATSCPP will beneficiate from pressure recovery due to diffuser tower shape in which flow stall doesn't occur.

The present study is based on the hypothesis that eddies dissipate part of the kinetic energy. As a result, pressure recovery is reduced [34]. A possible solution to deal with this problem and recover the amount of kinetic energy dissipated is using an ATSCPP instead of the cylindrical tower (CTSCPP) or DTSCPP to eliminate the apparition of eddies in the system. This consists of a power plant with an adapted annular tower in which the annular space guides the fluid flow. The schematic of the ATSCPP is shown in Fig. 2

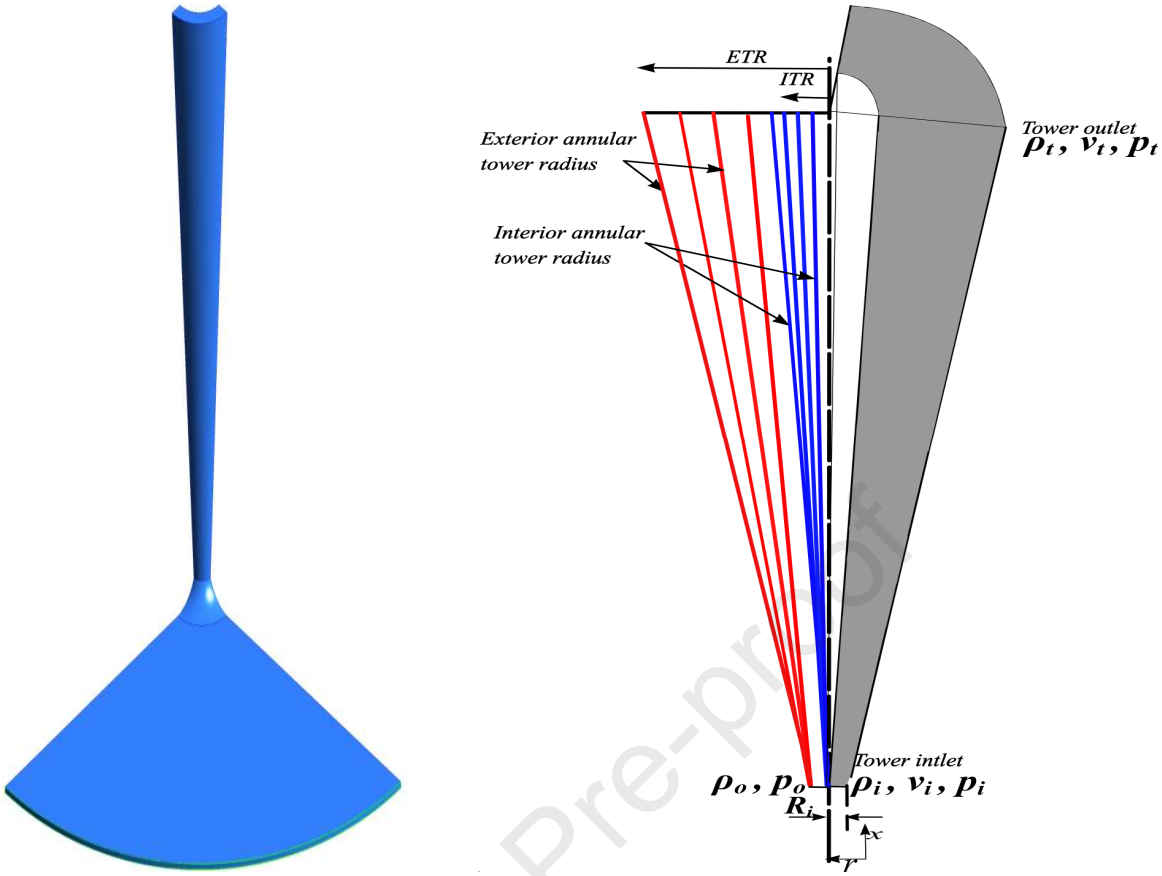

Fig. 2. Schematic of the ATSCPP.

The exterior and the interior tower walls were inclined to maximize energy generation. Therefore, Equation (2) representing the driving potential is rewritten as a function of the ETR and the ITR in Equation (4) to show how these geometric parameters can affect system performance.

The difference in the static pressure between the tower and the environment is given by [35]:

$$\Delta P = P_o - P_i \tag{1}$$

$$\Delta P = P_o - \left[P_t + \rho g H + \frac{1}{2}\left(\rho_t v_t^2 - \rho_i v_i^2\right) \right] \tag{2}$$

The static pressure at the tower outlet is given by:

$$P_t = P_o - \rho_0 g H \tag{3}$$

Substituting Equation (3) into Equation (2) and writing the ratio of the velocity of the tower top over the inlet. Thus the expression of driving potential can be expressed by:

$$\Delta P = (\rho_0 - \rho) gH + \frac{1}{2}\rho v_i^2 \left(1 - \left(\frac{R_i^2}{ETR^2 - ITR^2}\right)^2\right) \quad (4)$$

And based on the Boussinesq approximation:

$$\Delta P = \rho\beta\left(T_{ref} - T\right) gH + \frac{1}{2}\rho v_i^2 \left(1 - \left(\frac{R_i^2}{ETR^2 - ITR^2}\right)^2\right) \quad (5)$$

Where

$\rho\beta\left(T_{ref} - T\right) gH$ is the buoyancy force, and $\frac{1}{2}\rho v_i^2 \left(1 - \left(\frac{R_i^2}{ETR^2 - ITR^2}\right)^2\right)$ is the recovered pressure.

Equation (4) shows that the recovery due to diffuse like tower would reach the maximum with an optimal ETR and ITR values. So, an annular tower could be proposed as a solution to deal with this problem. A numerical study was carried out to show if this concept can bring a benefit to the system.

The ETR and ITR of the system are varied to study the effect of using an annular tower. The radius at the tower base was kept constant, and the other system dimensions were taken the same as the reference prototype case. Six configurations were studied numerically and were analyzed below. Configurations are presented in Table 3. For every configuration, the ETR was kept fixed where the ITR was varied until the area at the top of the tower became smaller and negatively affected the proposed concept. Simulations were performed in two cases, i.e., without load and with load using a turbine pressure drop selected from the data of the Spanish prototype, which belongs to 22-09-1985 at 12.00h.

Table 3

Configurations of the ATSCPPs.

Configuration	Tower	Tower inlet	ETR (m)	ITR (m)

	height	radius R_i (m)		
1	194.6	5.08	5.08	0[a]-2-3-4
2	194.6	5.08	9	0-3-5-7
3	194.6	5.08	13	0-3-5-7-9-11
4	194.6	5.08	17	0-3-5-7-9-11-13-15
5	194.6	5.08	21	0-3-5-7-9-11-13-15-17-19
6	194.6	5.08	23	0-3-5-7-9-11-13-15-17-19-21

[a] is also the base case

2.2. Numerical methods

The RANS-based two-equation k−w sst model has been used by many investigators to determine flow characteristics near the walls and boundary layer separation. For large ETRs, separating and secondary flows may take place in SC. So, the sst turbulence model is selected for this study. For more details on the model, the reader can consult the reference [38].

The governing equations that describe the steady, incompressible, and turbulent fluid flow inside the ATSCPP are given by:

Continuity equation:

$$\nabla \cdot \left(\rho \vec{v} \right) = 0 \tag{6}$$

Momentum equation:

$$\nabla \cdot \left(\rho \vec{v} \vec{v} \right) = -\nabla p + \nabla \cdot \left(\mu \left[\left(\nabla \vec{v} + \nabla \vec{v}^{T} \right) - \frac{2}{3} \nabla \cdot \vec{v} I \right] \right) - \rho \beta \left(T - T_{ref} \right) \vec{g} \tag{7}$$

Energy equation:

$$\nabla \cdot \left(\vec{v} \left(\rho E + p \right) \right) = \nabla \cdot \left(\lambda_{eff} \nabla T - h\vec{J} + \left(\mu \left[\left(\nabla \vec{v} + \nabla \vec{v}^{T} \right) - \frac{2}{3} \nabla \cdot \vec{v} I \right] \cdot \vec{v} \right) \right) + S_h \tag{8}$$

The transport equations for the *k−w sst* model are as follows [38]:

Turbulence kinetic energy transport equation:

$$\frac{\partial (\rho v_j k)}{\partial x_j} = G - \beta^* \rho \omega k + \frac{\partial}{\partial x_j} \left[\left(\mu + \sigma_k \mu_t \right) \frac{\partial k}{\partial x_j} \right] \tag{9}$$

Specific dissipation rate transport equation:

$$\frac{\partial (\rho v_j \omega)}{\partial x_j} = \frac{\gamma}{\nu_t} G - \beta \rho \omega^2 + \frac{\partial}{\partial x_j} \left[\left(\mu + \sigma_\omega \mu_t \right) \frac{\partial \omega}{\partial x_j} \right] + 2(1 - F_1) \frac{\rho \sigma_{\omega 2}}{\omega} \frac{\partial k}{\partial x_j} \frac{\partial \omega}{\partial x_j} \tag{10}$$

In which the turbulent eddy viscosity is computed from:

$$\mu_t = \frac{\rho a_1 k}{\max(a_1 \omega, \Omega F_2)} \tag{11}$$

Where

$$\Omega \equiv \sqrt{2 \Omega_{ij} \Omega_{ij}}$$

The model constants σ_{k1}, σ_{k2}, $\sigma_{\omega 1}$ and $\sigma_{\omega 2}$ are 0.85, 1, 0.5, 0.856, respectively (ANSYS, 2016). And β_1 =1, β_2 =0.09, κ=0.41, a_1=0.31.

A 3D geometry is created and meshed with a structured grid to deal effectively with the flow in the computational system using Gridgen pointwise 17.0. A study is carried out to get a suitable mesh that compromises between accuracy and computation time. A structured mesh was created, and four mesh sizes are considered to prove that the simulation results are independent of the mesh size. Grid sizes found are reported in Fig. 3. The selected 3D grid undergoes refinement near the exterior and interior tower surfaces since these regions play an

essential role in boundary layer investigation. The coarsest grid consists of 72 000 quadrilateral elements. Fig. 3 gives the results of sensitivity to the grid size. The relative static pressure was selected as the criterion of choice.

The results show that the optimal grid size is 552 000 elements (Grid 3) since the maximum difference between (Grid 3) and (Grid 4) was found to deviate by 0.1%. Thus, results from the third mesh can be considered grid-independent.

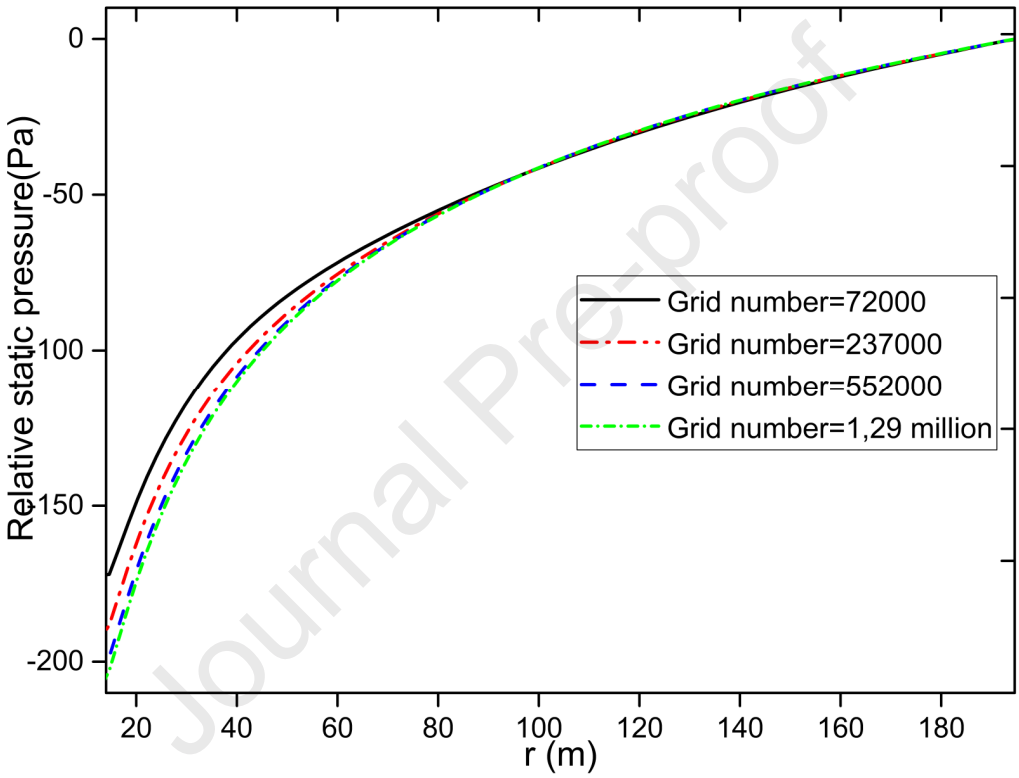

Fig. 3. Mesh independence study.

The selected grid is described in Fig. 4.

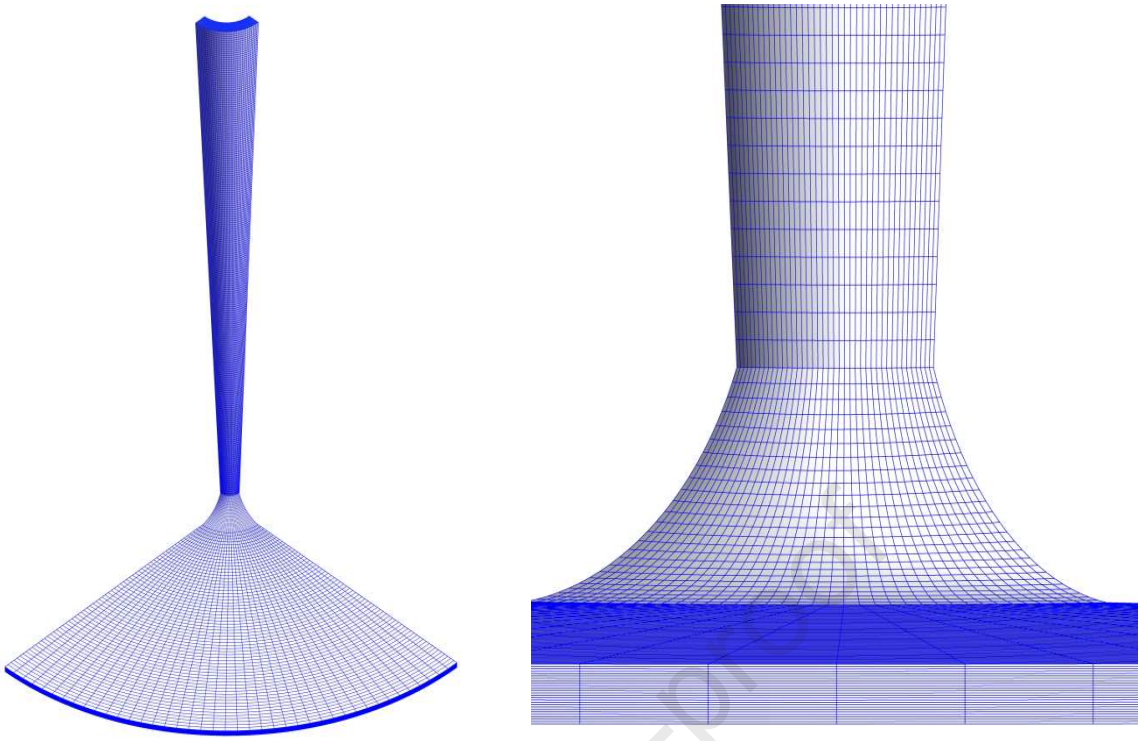

(a) (b)

Fig. 4. (a) Optimal mesh, (b) Part of the Optimal mesh.

The air properties have been taken in the same conditions of Spanish setup work. The temperature at the inlet was assumed constant and equal to 296 K. Static pressure at the inlet was taken equal to 93900 Pa. The heat flux at the ground was calculated, taking into consideration the collector efficiency. No-slip conditions are used for all solid walls. Two symmetry surfaces were used for the 3D model. The boundary conditions are shown in Fig. 5 and recapitulated in Table 4.

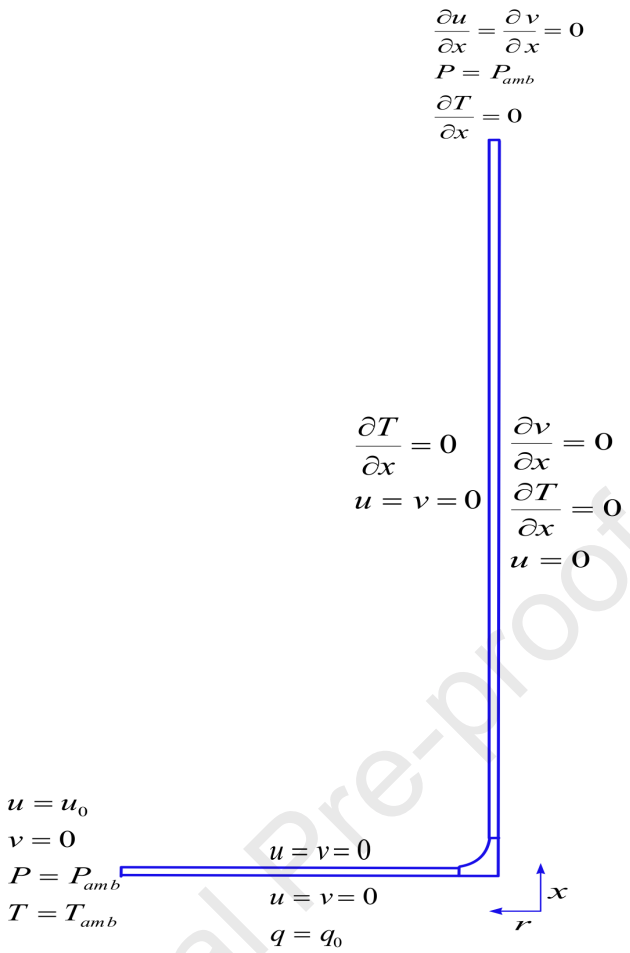

Fig. 5. Main boundary conditions.

Table 4

Boundary conditions.

Place	Type	Description
Collector surface	Wall	Adiabatic
Collector inlet	Pressure inlet	p = 93900 Pa
Collector outlet	Pressure outlet	p = 93900 Pa
Ground	Wall	Heat flux q
		$q = Qx\eta_c$ =245 W/m^{2a}
Tower surface	Wall	Adiabatic
Collector-to-tower transition section	Wall	Adiabatic

Turbine	Fan	Δp_{turb}= Constant value Δp_{turb}= 82.9 [a] Pa only for validation

[a] The data corresponds to midday of September the 2nd 1982 (Haaf, 1984), where global radiation was 844W/m^2 and collector efficiency was 0.29.

For the steady turbulent flow simulation, the ANSYS Fluent pressure-based solver was used. The SIMPLE algorithm is used for pressure-velocity coupling. The SIMPLE algorithm is a widely used numerical procedure to solve the Navier-Stokes equations for steady problems [3,11,13,28]. To compute the gradient of a given variable, the Least Squares Cell-Based is selected. For the computation of different variables, Second-Order Upwind Scheme is chosen. Using the turbulence model, the solver has to solve equations for turbulence, and then the convergence of the equation set is checked. This scheme is continued until the convergence criteria are fulfilled. A criterion of convergence for energy equation is set equal to 1×10^{-9} and 1×10^{-6} for other equations.

For more credibility, the model is first validated. The experimental data considered for validation represent different working hours on 2nd September 1982, (i.e., 10:00, 12:00, 14:00, 16:00) [35]. The updraft velocity, power output from the simulations are compared against the experimental data. Fig. 6 compares the updraft velocity and power output obtained from the simulation with experiment results. As shown in Table 5, the numerical results and experimental data of 2nd September 1982 compare quite well to each other with a small difference that can be noted. The maximum difference was roughly 13.87% in predicting the velocity and 12.67% in predicting the power output. This difference can be considered acceptable. Thus, numerical results would show well prediction in the flow dynamics.

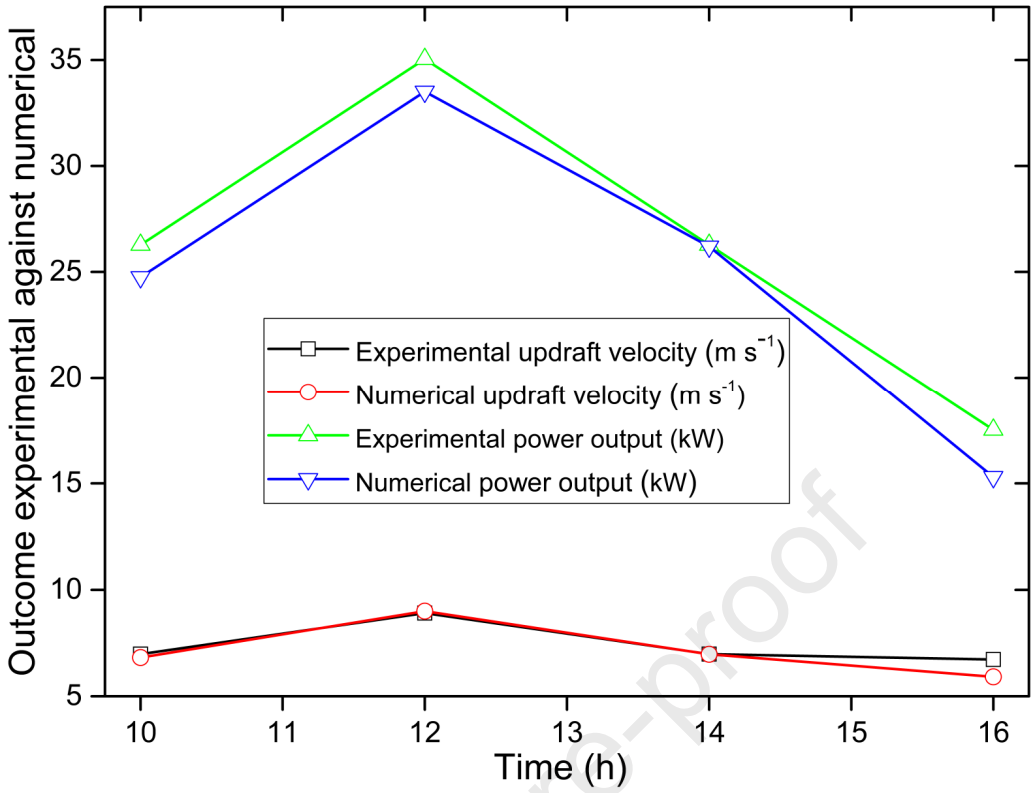

Fig 6. Updraft velocity and power output experimental against numerical results.

Table 5

Comparison of numerical results with experimental values.

Time (h)	radiation intensity	Updraft velocity (Experimental)	Updraft velocity (Calculated)	Deviation (%)	Power output (Experimental)	Power output (Calculated)	Deviation (%)
10h	746.15	6.98	6.82	2.29	26.28	24.76	5.78
12h	843.50	8.91	8.44	5.27	35.04	33.51	4.37
14h	741.80	6.98	6.97	0.14	26.28	26.20	0.30
16h	447.08	5.91	6.73	13.87	17.52	15.30	12.67

3. Results and discussion

This study investigates an annular tower concept that would overcome the boundary layer separation appearance in the divergent SC. Using the Spanish SC model, the influence of ETR and ITR on the SC performance were analyzed. Thus, the geometry of the proposed

model that maximizes power generation must be established. The simulations were carried out, considering two situations. The first doesn't incorporate the load (turbine). In a second step, the turbine is integrated into the system in order to evaluate with more precision the added value of the new concept. The turbine is treated as a disc using the fan model in Ansys Fluent. In the third part of this section, an ameliorated version of this new concept is proposed and examined.

3.1 Investigation of annular tower concept without load consideration

In this case, the load is not taken into consideration, and only flow pattern is investigated to examine the effect of the tower geometry on the flow. Fig. 7 shows the velocity streamlines within the tower of DTSCPP for different values of ETR. When the ETR is less than 13m, the airflow in one direction normal to the outlet surface, and the maximum velocity change shows a strong sensitivity to the change of ETR. When the ETR exceeds a specific value, the flow direction changes dramatically, and the reversal flow takes place. Once reversal flow is formed at the tower outlet, increasing ETR will enlarge the recirculation region. The backflow appearance leads to a decrease in the velocity. The phenomenon of boundary layer separation which manifests by secondary flows is responsible for the degradation of the driving potential. These observations confirm other researches results [33,34].

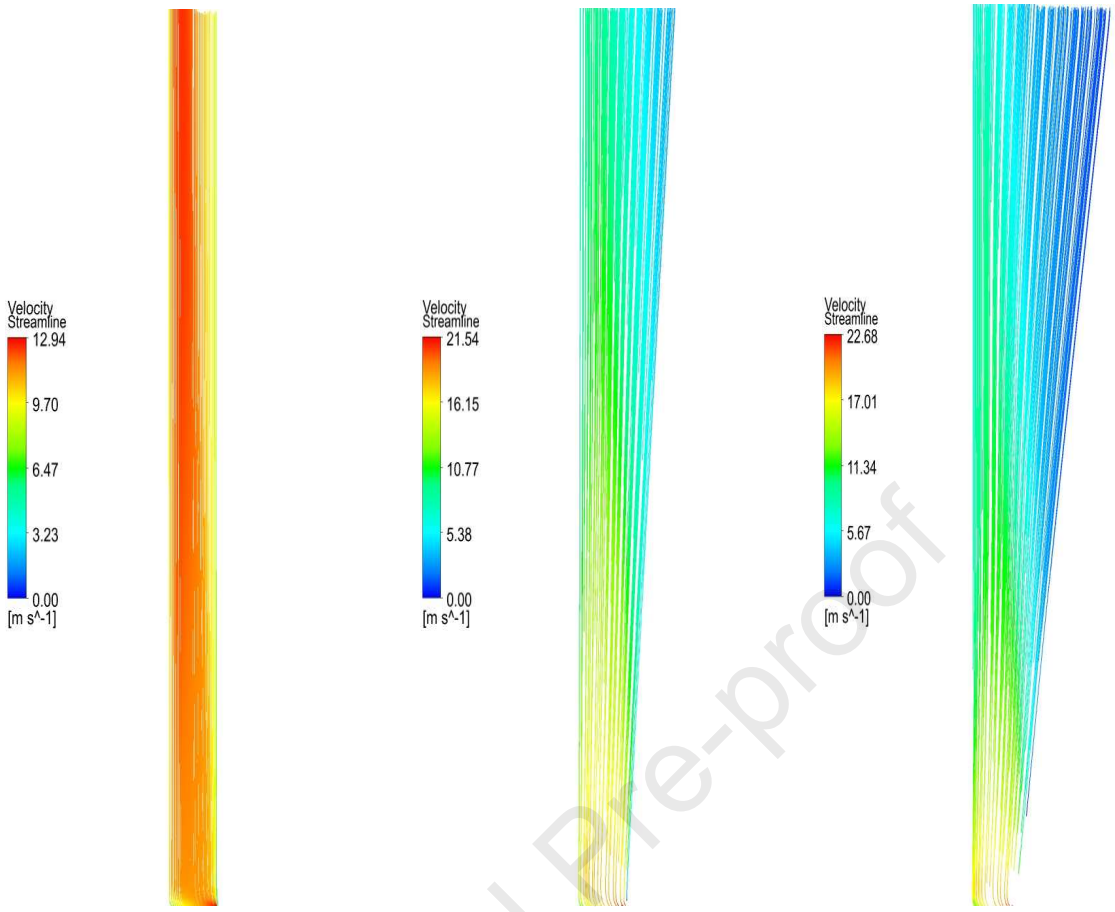

(a) (b) (c)

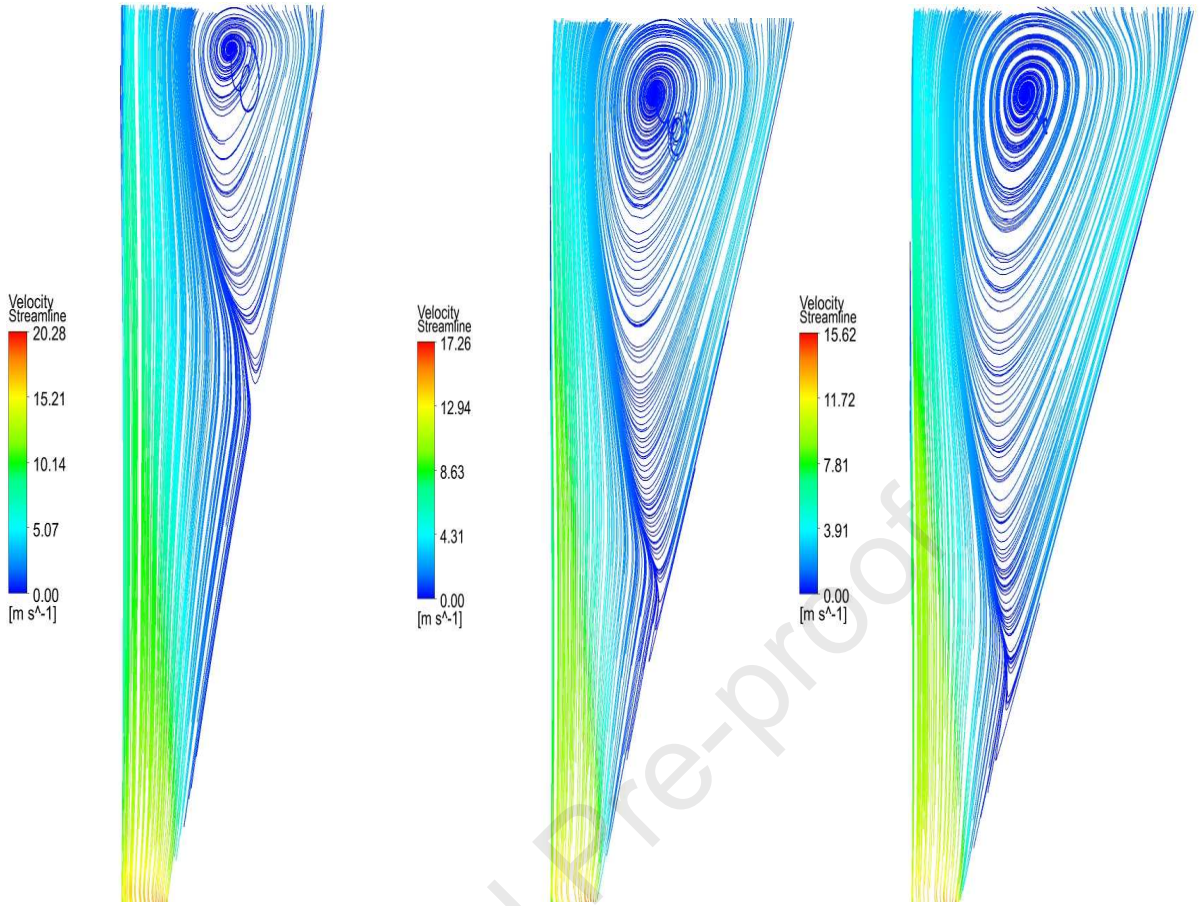

(d) (e) (f)

Fig. 7. Streamlines of DTSCPPs (ITR=0m) for different ETR values
(a) 5.08, (b) 9, (c) 13, (d) 17, (e) 21 and (f) 23

Adding a second tower wall to form the annular tower beneficiates from guiding the flow through the tower and minimizing the inverse effect of DTSCPP. In the case of higher ETRs, the ITR reduces the backflow intensity and enhances the flow acceleration as it moves in the annular space. This is shown in Fig. 8, which shows velocity path lines of ATSCPP (configuration ETR=21m) for different ITRs. Large-eddy formed and observed at the tower outlet is reduced with the increase of ITR and finally disappears. The decrease in the recirculation zone would result in kinetic energy recuperation.

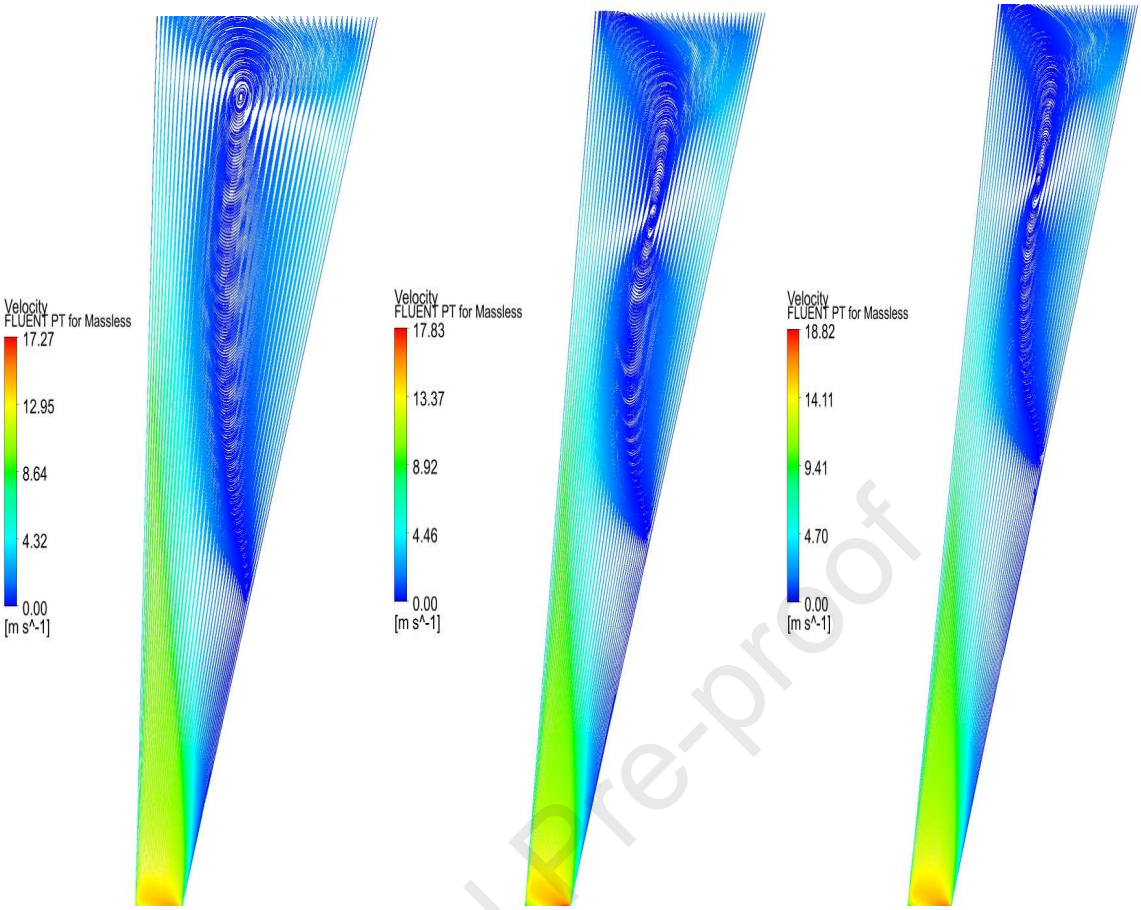

(a) 3m (b) 7m (c) 9m

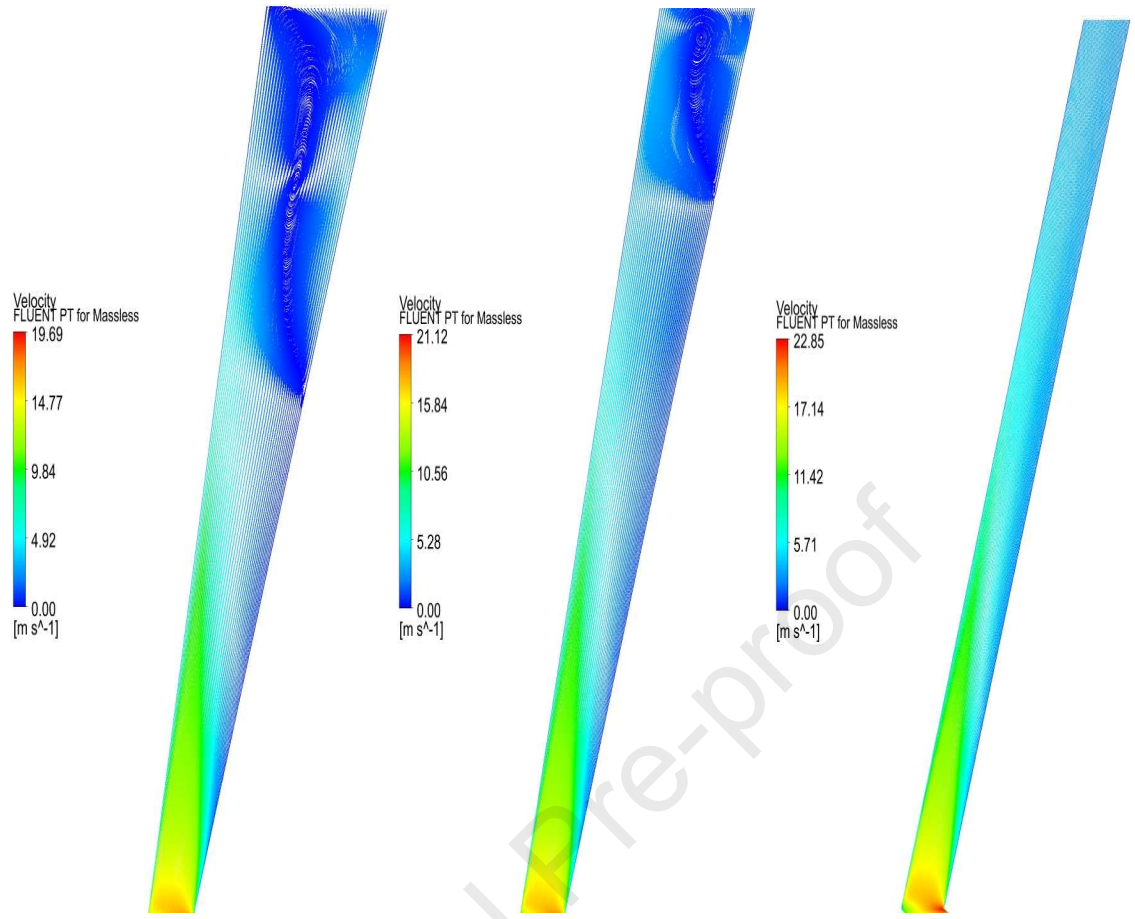

(d) 11m (e) 13m (f) 17m

Fig. 8. Velocity pathlines of annular SCPP (configuration ETR=21m) for different ITR : (a) 3m, (b) 7m, (c) 9m (d) 11m, (e) 13m and (f) 17m.

Fig. 9 gives more details on the effects of the annular tower on the flow. Fig. 9 shows the velocity vectors at the tower outlet for different values of ITR and same ETR (ETR=21m). Increasing the ITR decreases the backflow surface by approximately 40.00 % and increases the maximum velocity by 32.31 % (ITR=17 m).

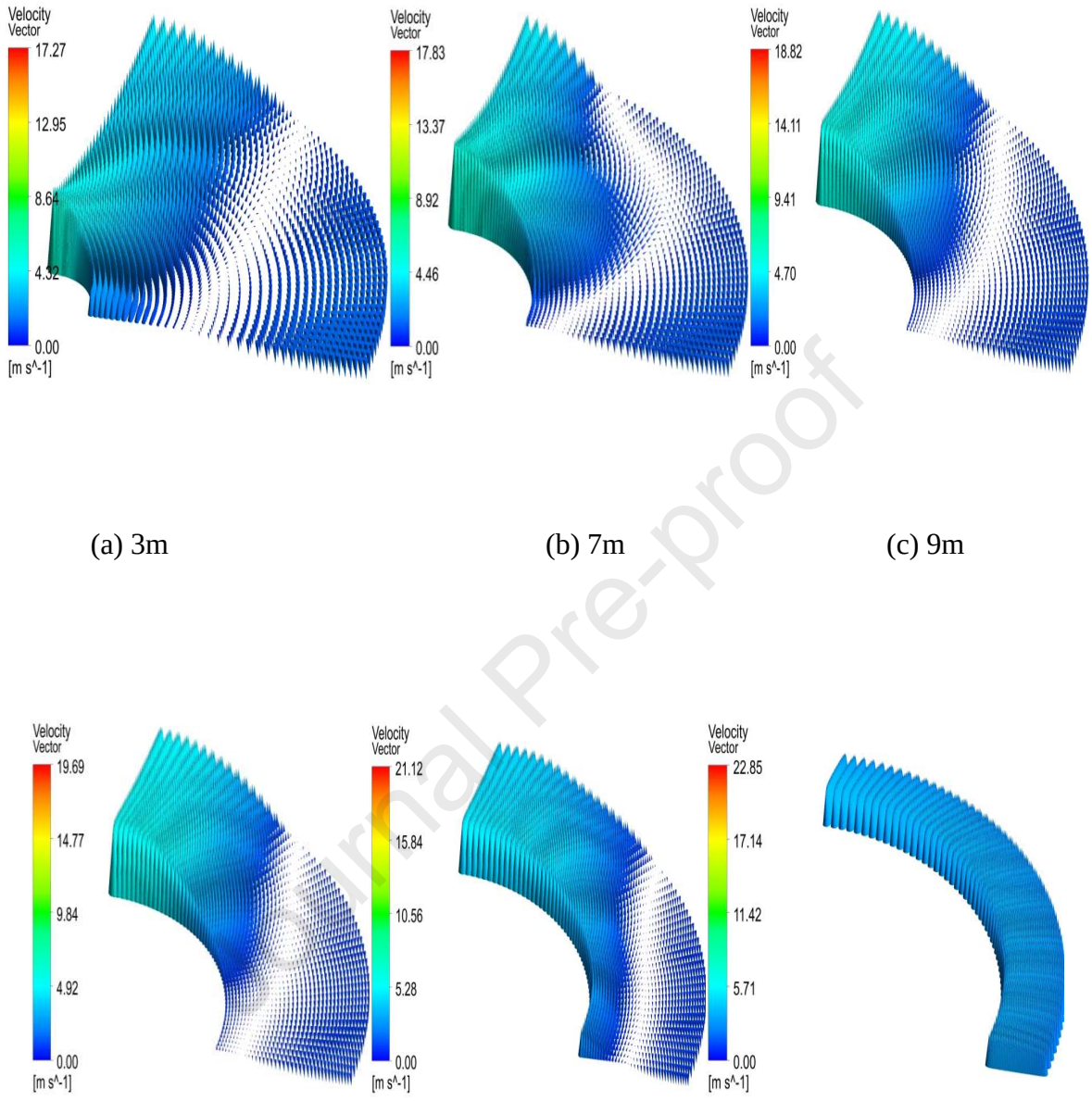

(a) 3m (b) 7m (c) 9m

(d) 11m (e) 13m (f) 17m

Fig. 9. Velocity vectors of annular SCPP (configuration ETR=21m) for different ITR : (a) 3m, (b) 7m, (c) 9m and (d) 11m, (e) 13m and (f) 17m.

When the boundary layer separation phenomenon occurs in the DTSCPP, the backflow will affect the temperature distribution negatively at the outlet, as shown in Fig. 10. The temperature rise increase with ETR increase. However, the average temperature decreases

from 309.2 K for an ETR of 5.08 m (base case) to 297.3 K for an ETR of 23 m. As a result, the buoyancy potential ($\rho\beta\left(T_{ref}-T\right)gH$) would decrease.

However, when using the ATSCPP, the temperature distribution at the outlet is more uniform (Fig.11), and the maximum temperature difference is about one degree for almost all cases. This value is less than that of the base case and higher compared with DTSCPP case. In the conventional SCPP, the driving potential is equal to buoyancy force only. In the DTSCPP, the potential recovery due to diffuser like a chimney is added to the system driving potential. However, in the ATSCPP, the system performs better potential recovery and higher buoyancy potential compared to the DTSCPP and the conventional system.

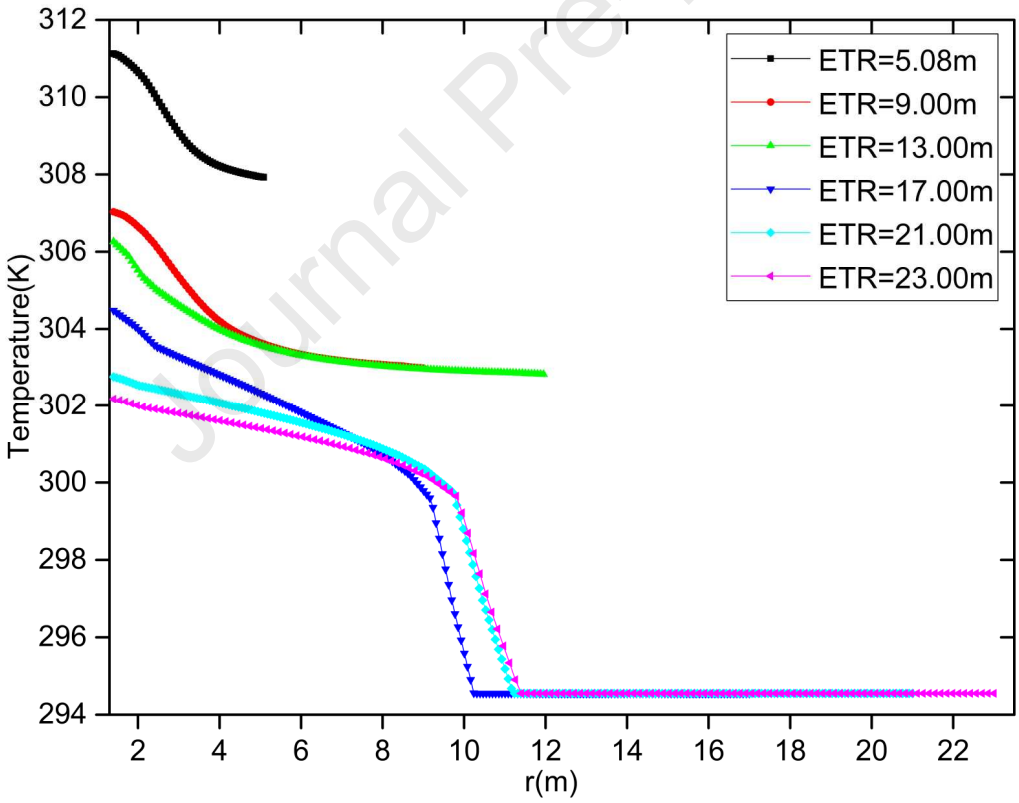

Fig.10. Temperature profile at the tower outlet for the DTSCPP.

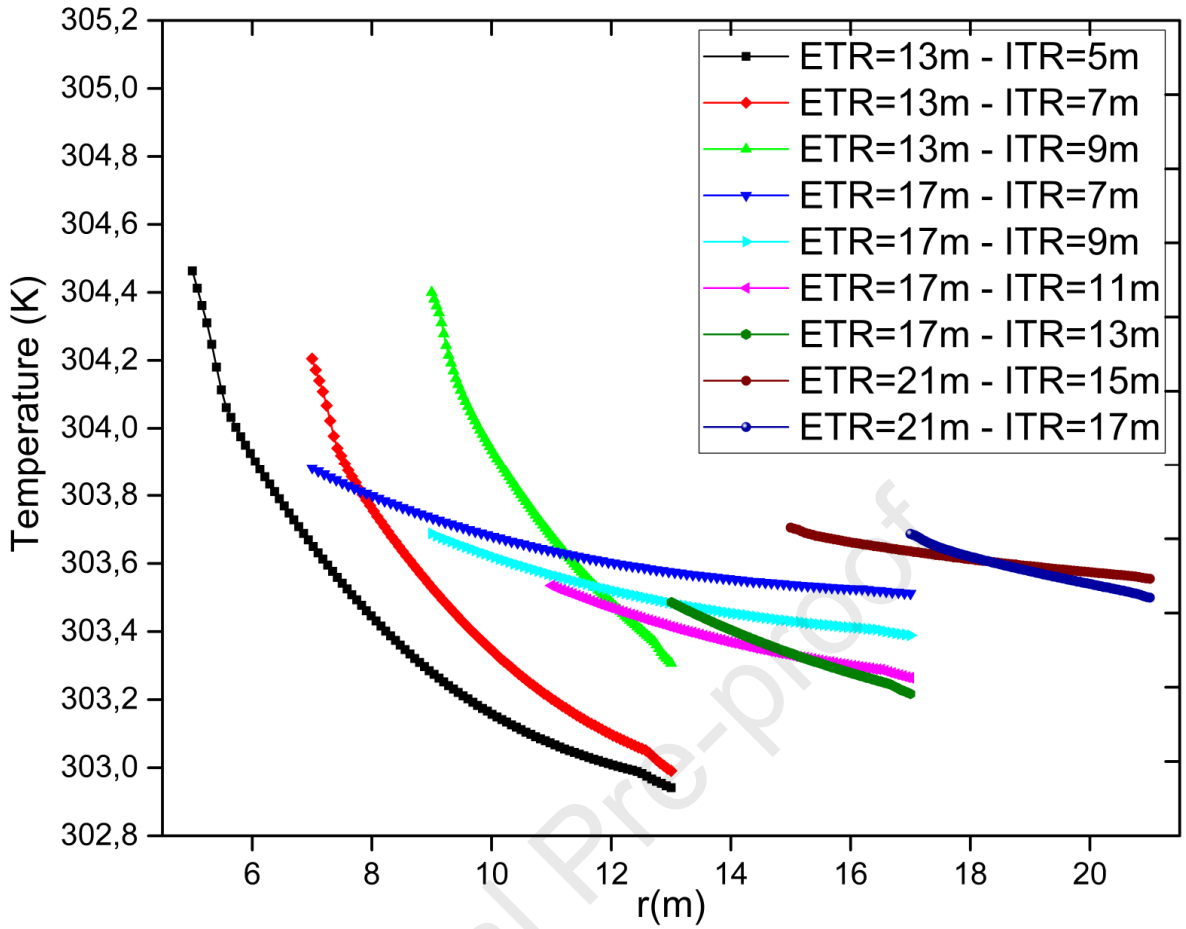

Fig.11. Temperature profile at the tower outlet for the ATSCPP.

The equation (4) shows that the driving potential is related to ITR and ETR values in such way that for an adequate ETR and ITR values, the buoyancy force and the pressure recovery would reach a maximum value as shown in Fig. 12. Fig. 12 shows how the ATSCPP alters the driving potential and as a result, affects the flow pattern inside the SC system. Compared with the base case (ITR=0m, ETR=5.08 m), all other configurations show higher static pressure. With a fixed ETR, when ITR varies, the recovered potential increases to reach a maximum value and then decreases owing to outlet surface obstruction and energy losses. In the DTSCPP, the backflow appearance near the tower outlet induces an important quantity of driving potential to lose, and thereby system performance degradation. However, the inverse effect is observed in the ATSCPP. In the ATSCPP, the increase in ITR for a fixed ETR affects the flow structure by decreasing the recirculation zone, resulting in recovering more pressure

than the two other cases (DTSCPP, CSCPP). The decrease in BLS makes the airflow free to move upward easily, in other words, velocity increases gradually with BLS decrease. The augmentation of velocity is not observed in the cases in which the flow recirculation occurred around the chimney exit. When both conditions are fulfilled, the disappearance of BLS, and the maximization of the tower outlet surface, the best case is obtained. Therefore, the best case is registered for an ATSCPP with ETR=17m and ITR=13m (Fig.13, 14).

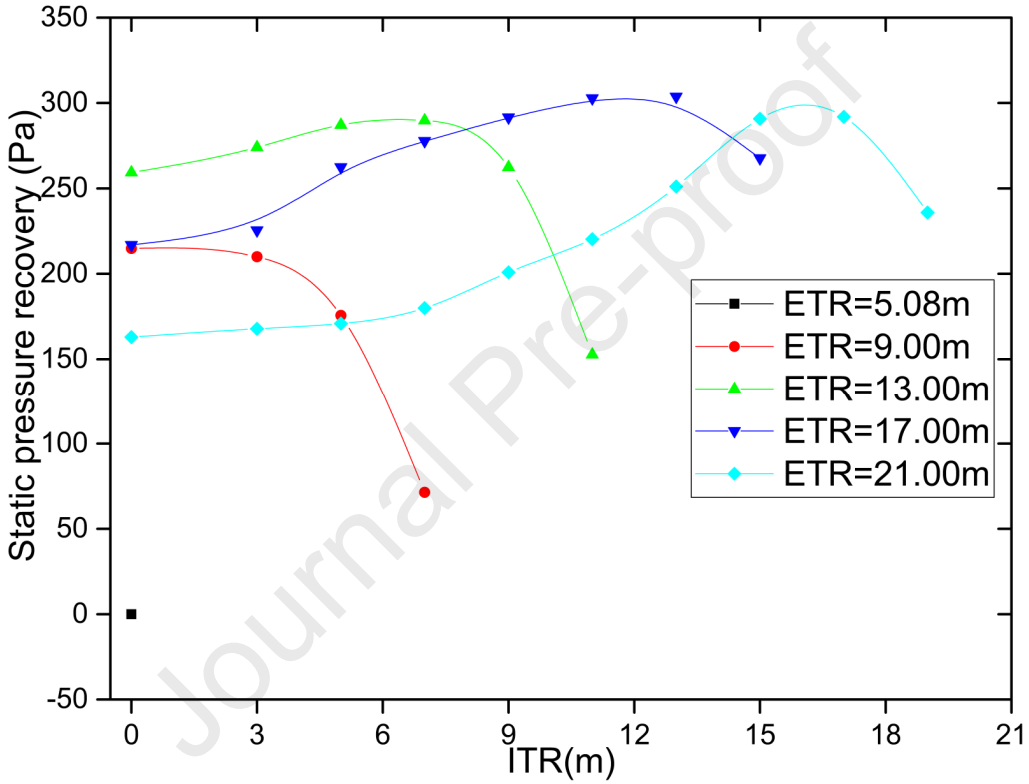

Fig. 12. Pressure recovery due to diffuser like chimney in case of ATSCPP (for different ETRs and ITRs).

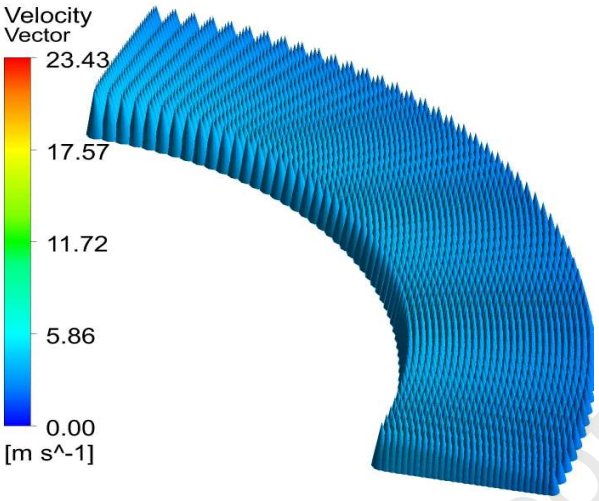

Fig. 13. Velocity vectors of annular SCPP (configuration ETR=17m, ITR=13).

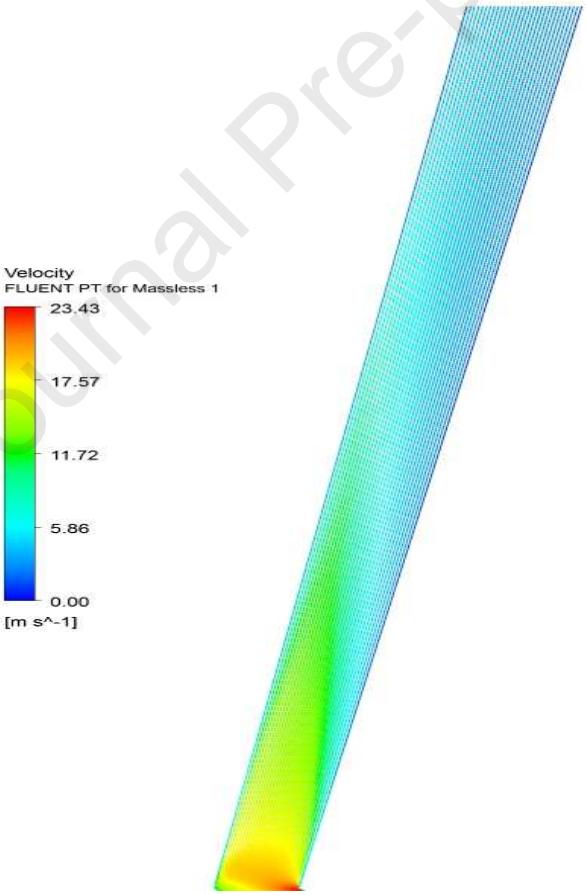

Fig. 14. Velocity pathlines of annular SCPP (configuration ETR=17m, ITR=13)

Fig. 15 shows the maximum velocity magnitude in the tower inlet and outlet for various ETRs. For the base case (ETR=5.08 m, ITR=0), there is no change in velocity values due to

the absence of recovered potential. For the other cases, the velocity at the outlet is less than its value at the inlet.

Getting a small difference in velocity magnitude at the tower inlet is not surprising because the aim is to decrease the velocity at the tower outlet and to increase the velocity at the tower inlet to enlarge the velocity difference $\left(\rho_t V_t^2 - \rho_i V_i^2\right)$ in eq.13, and as a result increasing the pressure recovery and the driving potential. Compared to the base case, a 76.15 % variation in the velocity at the tower inlet is noted and 41.64% variation is registered at the outlet when the DTSCPP is used. 82.29% variation is noted at the inlet and 74.85% variation at the outlet when the ATSCPP is used. Hence, the lost energy can be recovered using the annular tower SCPP. The proposed solution leads to convert the energy dissipated to static pressure. The best case is obtained for (ETR=17 m, ITR=13 m).

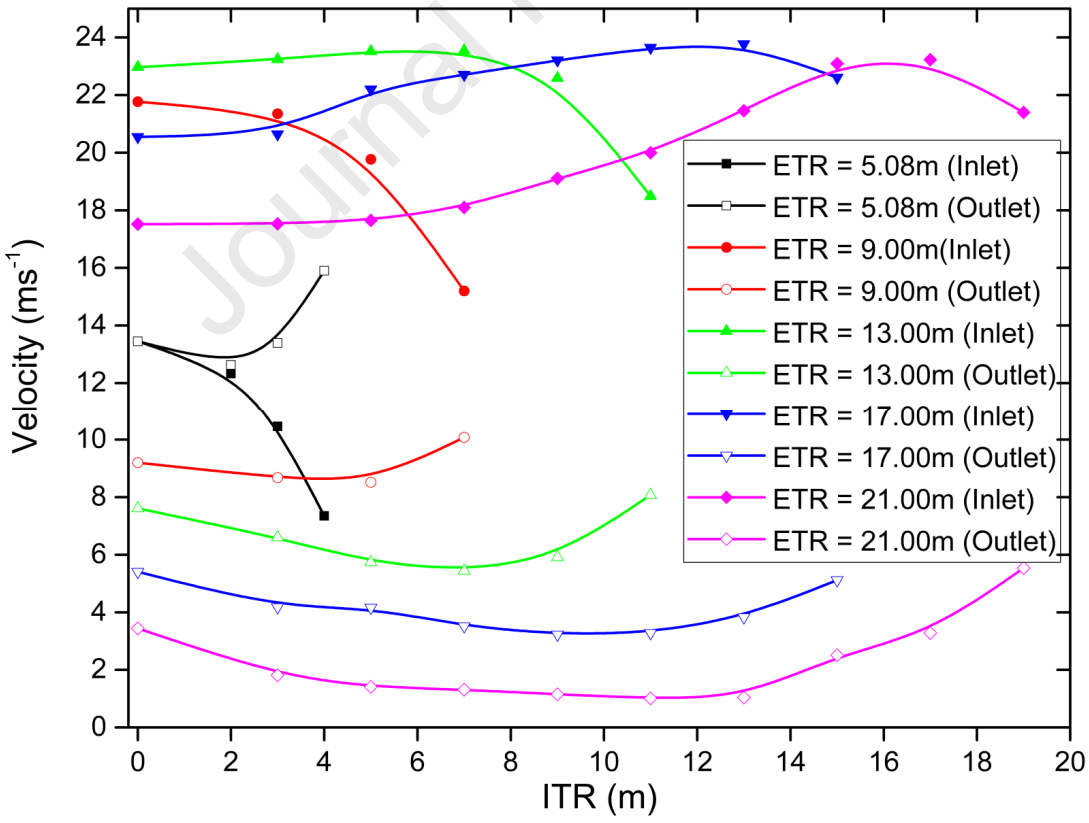

Fig. 15. Maximum velocity at the tower inlet and outlet.

3.2 Investigation of annular tower concept with load consideration

a. Flow pattern variations

In this section, flow characteristics in relation to thermal efficiency and power output are presented to confirm the results made earlier when considering the turbine. As seen in Fig. 16, the base case (cylindrical SC) shows small static pressure values. In the cylindrical SC, there was no static pressure recovered from the dynamic pressure, and thus only the buoyancy governed the inflow in the system. The Fig.16 also shows that diverging tower (for ETR < 17m) is more beneficial than the horizontal, but is still tangibly less beneficial. The favorable flow behavior inside the DTSCPP can be explained in the following way. In the divergent SCPPs, the recovered static pressure took a much larger proportion of the total driving potential relative to the buoyancy. The degradation in the system performance (for ETR >= 17m) was attributed to the boundary layer separation in the turbulent flow. This is a typical phenomenon in the flow within the diffusers known as diffuser stall. The diffuser stall is fundamentally a formation of small unsteady eddies separated from the diffuser walls. The stalls highly influence the recovery of static pressure, and the optimal recovery efficiency would be achieved when the first appreciable stall appears. Therefore using the appropriate ETR can increase the recovered static pressure significantly. It is important to notice that the recovered pressure change inside the system does not show a strong sensitivity to the change of ETR in case of using DTSCPP, as it does to the change of both ETR and ITR in case of using ATSCPP. ATSCPP beneficiate flow characteristics. Its results are better. Using the ATSCPP allows recovery of pressure in a large proportion of the total driving potential relative to buoyancy by decreasing the BLS. The decrease in BLS makes the airflow free to move upward quickly. Using the annular tower allows the static pressure to improve 44.44 % on the total.

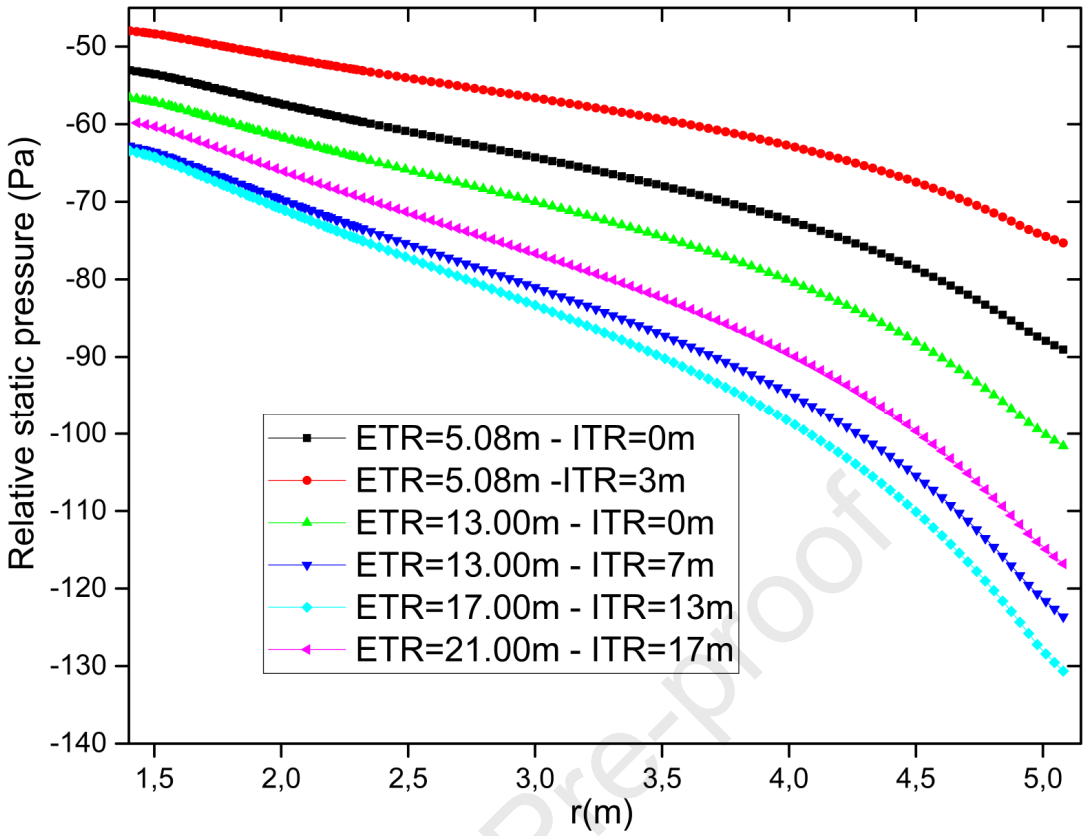

Fig. 16. Relative static pressure at the tower inlet.

The kinetic energy is transformed into pressure at the base of the tower. The static pressure is equivalent to the velocity. The more is the velocity; the less is the static pressure. The decrease in the static pressure for the annular tower is proof of its efficiency in decreasing BLS. The velocity at the tower outlet for the optimal ATSCPP configuration (ETR=17m, ITR=13) significantly makes the power output higher than that with either the diverging or the horizontal tower which confirms that the design of the solar tower is of great importance in the conception of SC. The total improvement in velocity magnitude equal to 32% (Fig. 17).

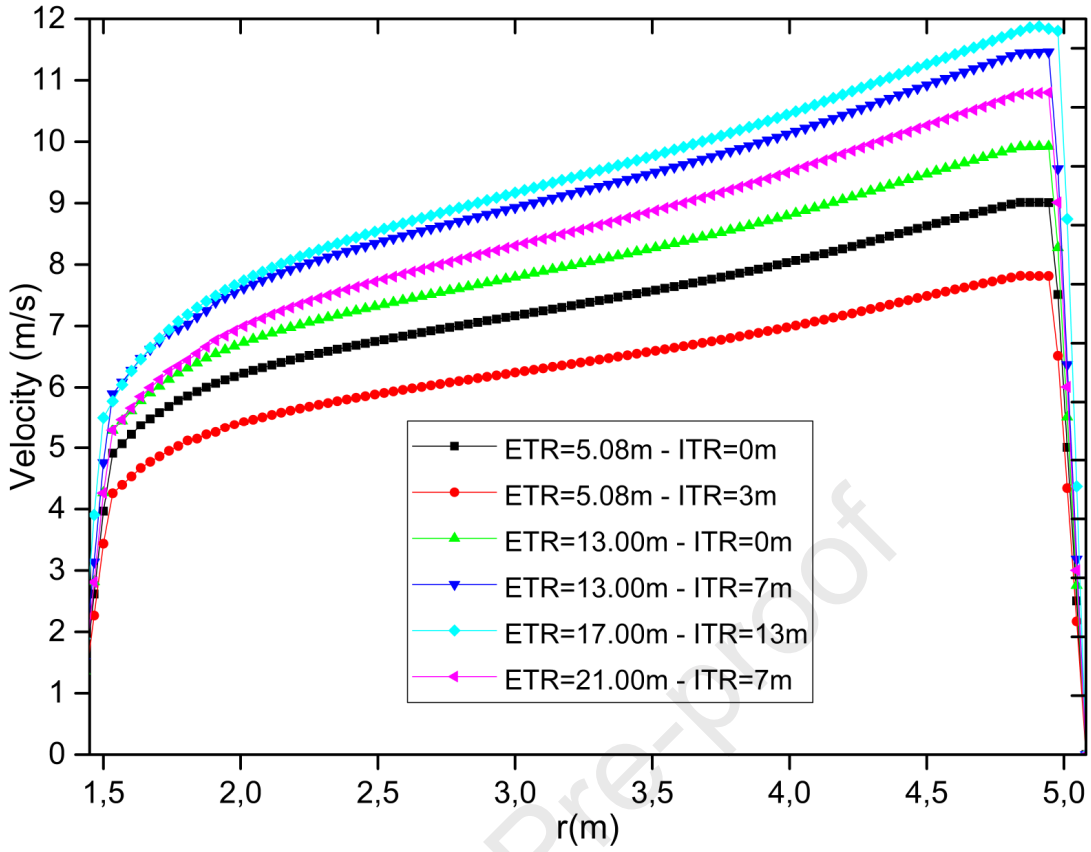

Fig. 17. Velocity profile at the tower inlet.

b. System performance

Comparisons of power output and thermal efficiency from different cases with the base case will give more indications about the improvement due to annular tower. Fig. 18 and Table 6 show power output compared to the base case. Higher power output could be achieved in the divergent chimneys. The divergent chimneys have an enhancement effect on the performance of SCPPs. However, the power output of divergent chimneys first increases until ETR=13m at which the peak power output is obtained. After that, the power output declines with further increasing the ETR, which may be caused by analogous tendencies in the driving potential and the velocity, which were also observed in other simulations. A similar tendency can be found in the power output of the annular tower. It would seem that there is an upper bound on ETR and ITR that can boost up the power. Too high ETR would eventually lead to BLS. As observed in the pressure and velocity plots, the 'proper'

combination between ETR and ITR offers the most significant power. It was found that the 'proper' combination remains the same (ETR=17, ITR=13) when considering the turbine load. This finding confirms that the airflow structure and BLS phenomenon is exclusively related to the solar tower geometry and not affected by turbine load.

Eqs. (12) and (13) are used to calculate the turbine power output and collector efficiency, respectively.

Turbine power output and system thermal efficiency can be calculated using Eqs. (12) and (13) respectively [39,40]:

$$P = \eta_t \Delta p_{turb} Q_v \tag{12}$$

$$\eta = \frac{(T_1 + \Delta T)}{\Delta T}\left[1 - \left(1 - \frac{\Delta P_{turb}}{P_1}\right)^{\frac{\kappa-1}{\kappa}}\right] \tag{13}$$

Where

The turbine efficiency was set as 0.8 [40-42].

Table 6

Power output for different ITR and ETR values.

Case	Updraft velocity ($m.s^{-1}$)	Power output (kW)	Difference (%)
ETR=5,ITR=0[a]	9.00	33.51	-
ETR=5, ITR=3	7.81	29.08	13.22
ETR=13, ITR=0	9.92	36.93	10.21
ETR=13, ITR=7	11.46	42.66	27.31
ETR=17, ITR=13	11.88	44.23	32.00
ETR=21, ITR=17	10.80	40.21	20.00

[a] is also the reference case

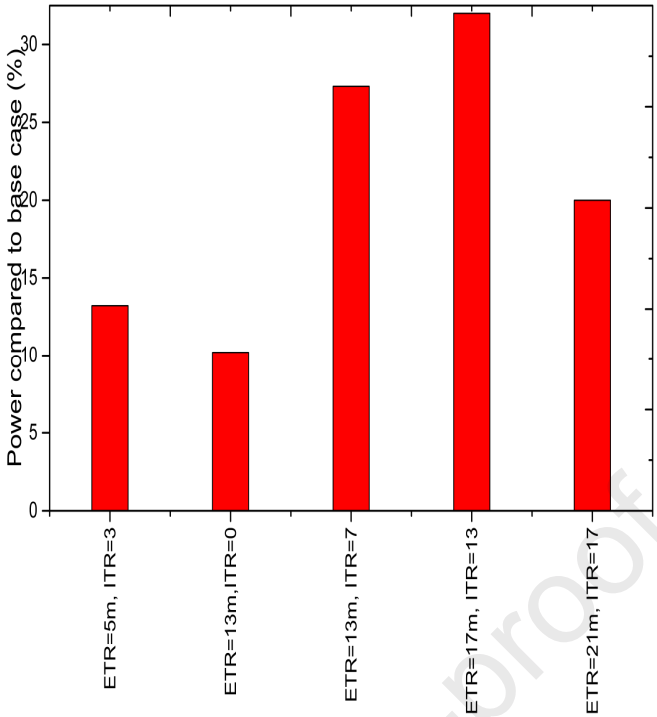

Fig. 18. Power output compared to the base case.

Temperature profile through the collector is shown in Fig. 19 to better understand the effect of the annular tower on the thermal efficiency of the SC. It should be noticed that the temperature rise, ΔT, in the divergent-SC and ATSCPP systems is always less than that in the cylindrical SCPP. Besides, Fig. 19 shows a contrary trend relative to the velocity: ΔT decreased from 20.31 K (base case) to a minimum of 16.98 K (at ETR=17m, ITR=13). The energy balance could explain this result at the ground boundary where the fixed solar insolation resulted in a decrease in ΔT due to the system's growth of velocity. The slight temperature rise indicates higher thermal efficiency, as shown in Fig. 20 and Table 7. If we note that the modification in the SCPP system is purely physical, the total improvement can be considered promising in energy production with this type of system.

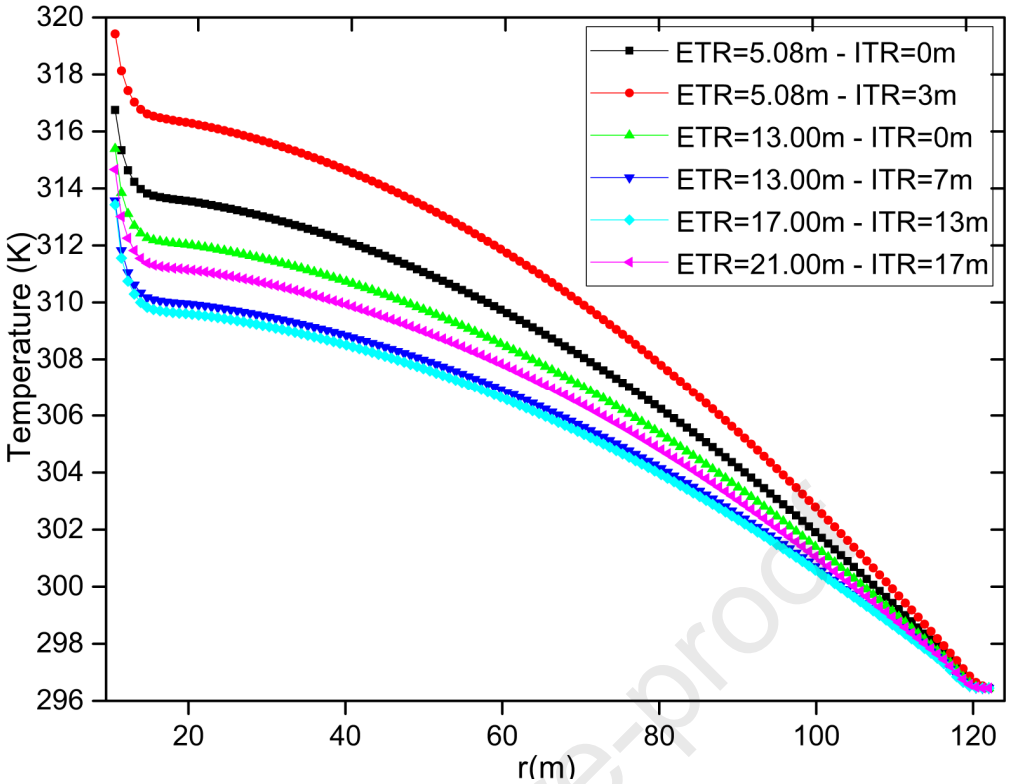

Fig. 19. Temperature profile through the collector.

The values of temperature rise are consistent with the efficiency presented in Fig. 20. Thermal efficiency depends on temperature rise, as seen in Eq (13). A lower temperature rise should give higher efficiency. The maximum deviation between the obtained optimum case and the benchmark case exceeds 20%.

Table 7

SCPP system thermal efficiency.

Case	ΔT	η (%)	Difference (%)
ETR=5, ITR=0[a]	20.31	0.39	-
ETR=5, ITR=3	22.97	0.35	11.43
ETR=13, ITR=0	18.94	0.42	07.69
ETR=13, ITR=7	17.13	0.46	17.95
ETR=17, ITR=13	16.98	0.47	20.51
ETR=21, ITR=17	18.22	0.44	12.82

[a] is also the reference case

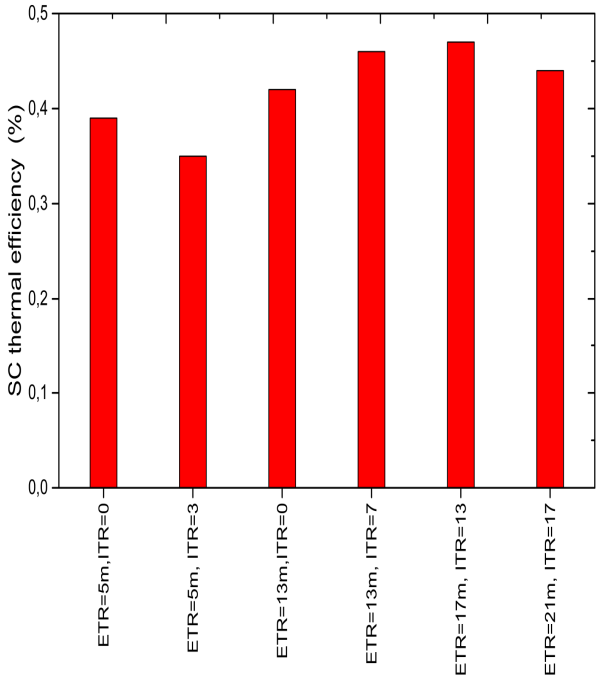

Fig. 20. (a) System thermal efficiency

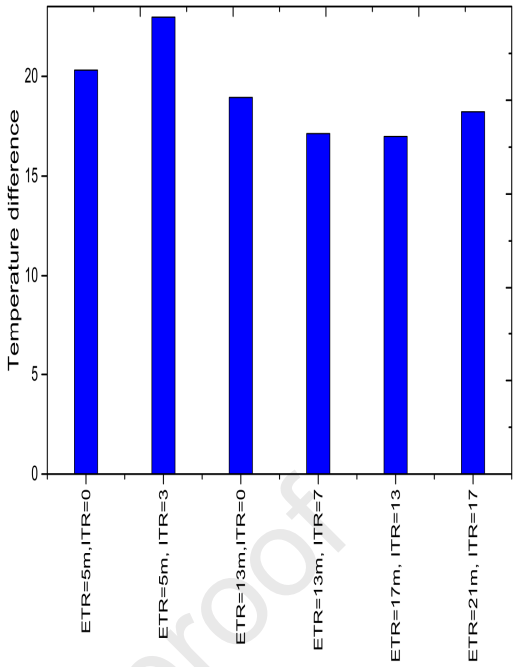

Fig. 20. (b) Temperature difference.

3.3 Investigation of an improved annular tower concept

In this section, a controlling method of the airflow characteristics inside the SC tower is introduced. Since the annular tower provides a promising approach for energy supply, but adding a second tower wall leads to increase construction costs. Then, a compromise between power generation and induced costs expressed by total tower surface is needed. The idea is to propose an interior tower wall with an adequate height to be applied in the region in which, the eddies appear, to control the outflow passively as shown in Fig. 21. Taking the optimal case (ETR=17, ITR=13 m) as the reference, the power output of SC varied from 44.23 kW to 41.55 kW when the height of the interior tower wall is reduced from 185 m to 4.9 m (Table 8). The maximum difference in power output between controlled tower outflow and the annular tower is only 6% compared to the significant decrease in the cost expressed by the total surface of tower walls (40%) (Fig.22).

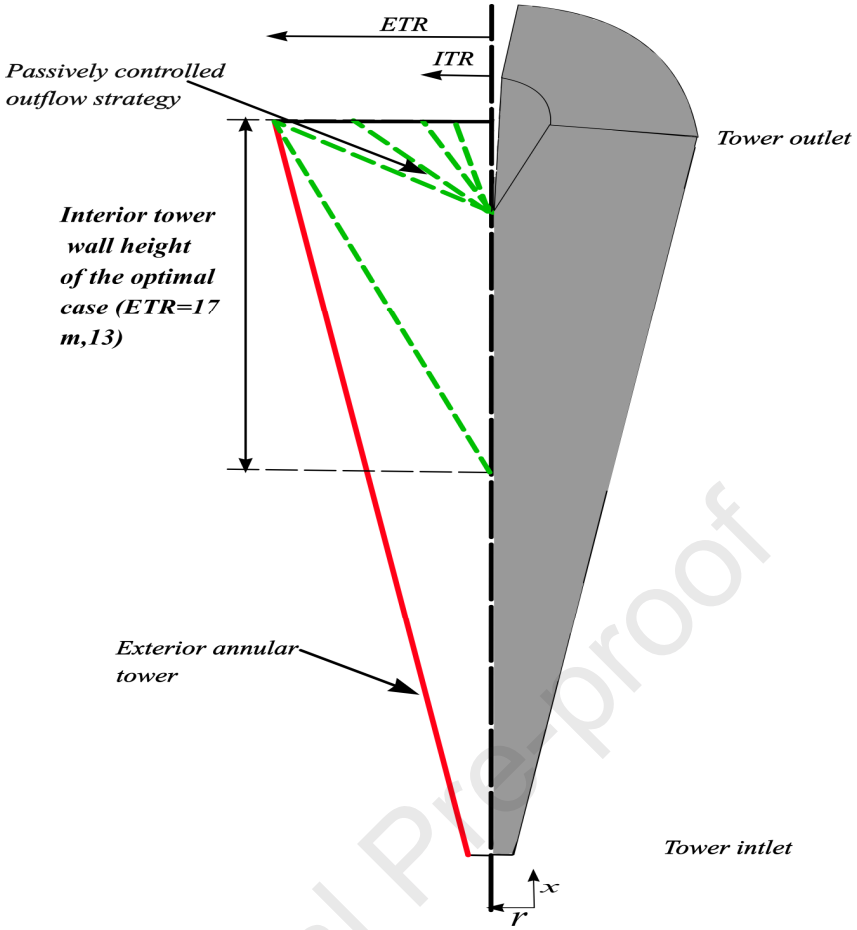

Fig. 21. Schematic of the ATSCPP with passively controlled outflow.

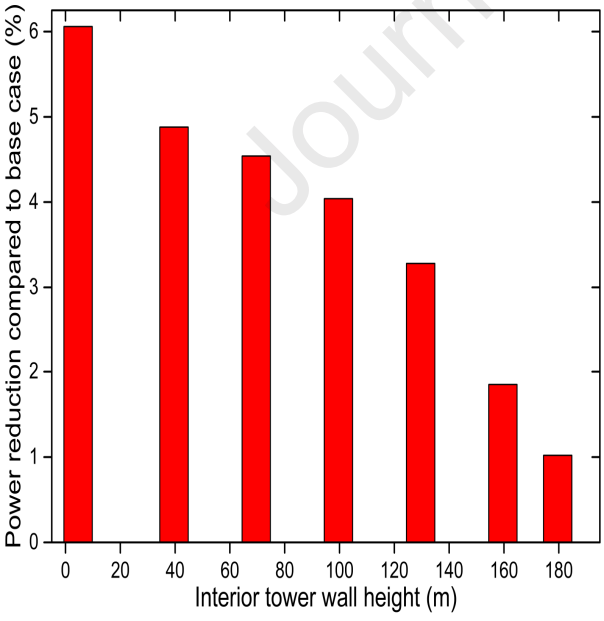

Fig. 22. (a) Power reduction for different interior tower wall height (ETR=17,ITR=13m)

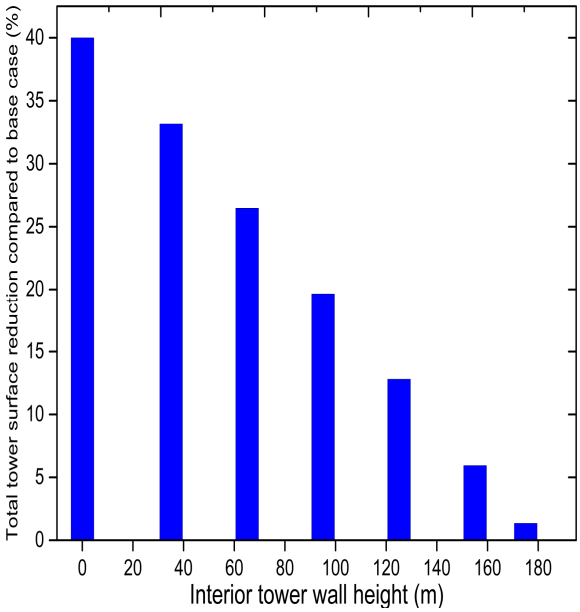

Fig. 22. (b) Cost variation for different interior tower wall height (ETR=17,ITR=13)

Table 8

Power output of the case (ETR=17, ITR=13 m) for different interior tower wall height (m).

Interior tower wall height of the optimal case (m)	Updraft velocity (m/s)	Power (kW)	Difference (%)	Total surface of tower walls (m^2)	Difference (%)
4.6	11.16	41.55	6.06	10734.48	40.00
9.6	11.22	41.77	5.56	10831.29	39.03
39.6	11.30	42.07	4.88	11873.50	33.16
69.6	11.34	42.22	4.54	13062.96	26.47
99.6	11.40	42.44	4.04	14273.52	19.66
129.6	11.49	42.78	3.28	15490.81	12.81
159.6	11.66	43.41	1.85	16711.05	5.94
179.6	11.76	43.78	1.02	17525.47	1.35
185.6[a]	11.88	44.23	-	17766.04	

[a] Taken as the reference case.

Conclusion

The present study consists of an investigation of a new solar chimney tower concept that would overcome eddies creation in the conventional system. Based on the obtained results, the following conclusions can be drawn:

- Higher tower diverging angles are responsible for eddies generation and static pressure reduction, and thereby SC performance degradation.
- Flow behavior, power output, and thermal efficiency show a strong sensitivity to the change of both ETR and ITR. The best case is obtained when (ETR=17m, ITR=13m).
- The new SCPP concept proposed, namely ATSCPP, allowed a significant increase in the driving potential. The total improvement in power output equal to 32%.
- The outflow control approach is more effective. The proposed method can significantly reduce tower costs. Total tower surface is reduced by 40%, whereas the power is reduced by only 6.06%.

Nomenclature

amb	ambient
E	total energy (J)
F_1, F_2	blending functions
G	generation of turbulence kinetic energy (J/m^3.s)
g	gravity constant (m/s^2)
H	chimney height (m)
H_{ci}	Collector inlet height (m)
H_{co}	Collector outlet height (m)
H_{wt}	Wind turbine height (m)
h	Wind turbine height (H_{wt})
I	unit tensor
J	diffusion flux of species j
P	pressure (Pa)
P_i	pressure inside the tower (Pa)
P_t	pressure at the top of the tower (Pa)
P_0	pressure outside the tower (Pa)
P_1	pressure at the collector inlet (Pa)
Q_v	volume flow rate (m^3/s)
q	solar radiation (W/m^2)
q_o	heat flux (W/m^2)
R_c	Collector radius (m)
R_i	tower inlet radius (m)
R	Tower radius (m)
r	coordinate in radial direction (m)
ref	reference
S_h	Source term
T	temperature (K)
T_1	temperature at the collector inlet (K)
turb	turbine
u	air velocity in axial direction (m/s)
u_0	initial air velocity in axial direction (m/s)
v	air velocity in radial direction (m/s)
x	coordinate in axial direction (m)

Acronyms

ATSCPP	annular tower solar chimney power plant
BLS	boundary layer separation
CFD	computational fluid dynamics
CTSCPP	conventional tower solar chimney power plant
DTSCPP	divergent tower solar chimney power plant
ETR	exterior tower radius (m)
ITR	interior tower radius (m)
NS	Navier Stokes
PV	photovoltaic

RANS	Reynolds Averaging Navier-Stokes
RSM	response Surface Methodology
SC	solar chimney
SCPP	solar chimney power plant
SIMPLE	Semi-Implicit Method for Pressure- Linked Equations
3D	three-dimension

Greek symbols

β	volume coefficient of expansion (1/K)
Δ	difference
Δp_{turb}	pressure drop across the turbine (Pa)
ΔT	temperature rise (K)
η	thermal efficiency (%)
η_t	turbine efficiency (%)
k	turbulent kinetic energy (J/kg)
κ	specific heat ratio
λ_{eff}	effective heat conduction coefficient
μ	fluid dynamic viscosity (kg/m.s)
μ_t	dynamic eddy viscosity (kg/ms)
ν_t	kinematic eddy viscosity (m^2/s)
ρ	air density (kg/m^3)
Ω_{ij}	mean rate-of-rotation tensor
w	specific dissipation rate

References

[1] World Energy Council World, Energy Issues Monitor 2019 https: //www. worldenergy. org/publications/entry/world-energy-issues-monitor-2019-managing-the-grand-energy-transition.

[2] International Energy Agency, Global EV Outlook 2019 https: //www. iea. org/publications/reports/globalevoutlook2019/.

[3] Abdeen A, A. Serageldinc A, Ibrahima M., El-Zafaranyd A, Ookawarae S, Muratae R. Solar chimney optimization for enhancing thermal comfort in Egypt: An experimental and numerical study. Solar Energy 2019;180:524-536.

[4] Jafarifar N, Behzadi M M, Yaghini M. The effect of strong ambient winds on the efficiency of solar updraft power towers: A numerical case study for Orkney. Renewable Energy 2019;136:937-944.

[5] Mahmoudimehr J, Sebghati P. A Novel Multi-objective Dynamic Programming Optimization Method: Performance Management of a Solar Thermal Power Plant as a Case Study, Energy (2018), doi: 10.1016/j.energy.2018.11.079

[6] Pritam Das, Chandramohan V. Computational study on the effect of collector cover inclination angle, absorber plate diameter and chimney height on flow and performance parameters of solar updraft tower (SUT) plant. Energy 2019;172:366-379.

[7] Aligholamia, Shiva Sh, Khosroshahib, Alireza R. Khosroshahia. Hydrodynamic and thermodynamic enhancement of a solar chimney power plant. Solar Energy 2019;191: 180-192.

[8] Belkhode P, Sakhale C, Bejalwar A. Evaluation of the experimental data to determine the performance of a solar chimney power plant, Materials Today: Proceedings, https://doi.org/10.1016/j.matpr.2019.09.006

[9] Hussain H, Al-Kayiem, Mohammed A, Aurybi, Syed I.U, Gilani, Ali A, Ismaeel, Sanan T. Mohammad. Performance Evaluation of Hybrid Solar Chimney for Uninterrupted Power Generation, Energy (2018), doi: 10.1016/j.energy.2018.10.115

[10] Amudam Y, Chandramohan VP, Influence of thermal energy storage system on flow and performance parameters of solar updraft tower power plant: A three dimensional numerical analysis, *Journal of Cleaner Production* (2018), doi: https: //doi. org/10. 1016/j.jclepro.2018.09.248.

[11] Attig-Bahara F, Sahraouib M, Guellouzd M S, Kaddechef S. Effect of the ground heat storage on solar chimney power plant performance in the South of Tunisia: Case of Tozeur. Solar Energy 2019;193:545-555.

[12] Fallah S H, Valipour M S. Evaluation of solar chimney power plant performance: The effect of artificial roughness of collector. Solar Energy 2019;188:175-184.

[13] Haghighat S, Kasaeian A, Pourfayaz F, Shahdost B M. Fluid dynamics analysis for different photovoltaic panel locations in solar chimney. Energy Conversion and Management 2019;191:71-79.

[14] Li G, Huang H, Zhangb J, Zhangc H. Study on the performance of a solar collector with heat collection and storage. Applied Thermal Engineering 2019;147:380-389.

[15] Jamali S, Nemati A, Mohammadkhani F, Yari M. Thermal and economic assessment of a solar chimney cooled semitransparent photovoltaic (STPV) power plant in different climates. Solar Energy 2019;185:480-93.

[16] Habibollahzade A. Employing photovoltaic/thermal panels as a solar chimney roof: 3E analyses and multi-objective optimization, Energy (2018), doi: 10.1016/j.energy. 2018.10.048

[17] Kebabsa H, Lounici M S, Lebbi Mohamed, Daimallah A. Thermo-hydrodynamic behavior of an innovative solar chimney. Renewable Energy 2020;145:2074-2090.

[18] Li J-y, Guo P-h, Wang Y. Effects of collector radius and chimney height on power output of a solar chimney power plant with turbines. Renewable Energy 2012;47:21-28.

[19] Balijepalli R, Chandramohan V.P, Kirankumar K. Optimized design and performance parameters for wind turbine blades of a solar updraft tower (SUT) plant using theories of Schmitz and aerodynamics forces. Sustainable Energy Technologies and Assessments 2018;30:192-200.

[20] Von Backstrom T W, Gannon A J. Solar chimney turbine characteristics. Solar Energy 2004;76:235-241.

[21] Fluri T.P, von Backstrom T W. Comparison of modelling approaches and layouts for solar chimney turbines. Solar Energy 2008;82:239-246.

[22] Fluri T.P, von Backstrom T W. Performance analysis of the power conversion unit of a solar chimney power plant. Solar Energy 2008;82:999-1008.

[23] Denantes F, Bilgen E. Counter-rotating turbines for solar chimney power plants. Renewable Energy 2006;31:1873-1891.

[24] Nizetic S, Klarin B. A simplified analytical approach for evaluation of the optimal ratio of pressure drop across the turbine in solar chimney power plants. Applied Energy 2010;87:587-591.

[25] Guo P, Li J, Wang Y, Guo Y W. Evaluation of the optimal turbine pressure drop ratio for a solar chimney power plant. Energy Conversion and Management 2016;108:14-22.

[26] Guo P, Li J, Wang Y, Liu Y

. Numerical analysis of the optimal turbine pressure drop ratio in a solar chimney power plant. Solar Energy 2013;98:42-48.

[27] Zhou X, Yang J, Xia B, Hou G, Xing F. Analysis of chimney height for solar chimney power plant. Applied Thermal Engineering 2009;29:178-185.

[28] Shirvan KM, Mirzakhanlari S, Mamourian M, Abu-Hamdeh Nidal. Numerical investigation and sensitivity analysis of effective parameters to obtain potential maximum power output: A case study on Zanjan prototype solar chimney power plant. Energy Conversion and Management 2017;136:350-360.

[29] Ming TZ, Richter RK, Meng F. Chimney shape numerical study for solar chimney power generating systems. International Journal of Energy Research 2013;37:310-322.

[30] Okada S, Uchida T, Karasudani T, Ohya Y. Improvement in Solar Chimney Power Generation by Using a Diffuser Tower, Journal of solar energy engineering, doi: 10.1115/1.4029377.

[31] Koonsrisuk A, Chitsomboon T. Effects of flow area changes on the potential of solar chimney power plants. Energy 2013;51:400-406.

[32] Patel SK, Prasad D, Ahmed MR. Computational studies on the effect of geometric parameters on the performance of a solar chimney power plant. Energy Conversion and Management 2014;77:424-431.

[33] Hu S. Numerical modelling and comparison of the performance of diffuser-type solar chimneys for power generation, Appl. Energy (2017), http: //dx. doi. org/10. 1016/j. apenergy.2017.03.040

[34] Xu Y, Zhou X. Performance of divergent-chimney solar power plants. Solar Energy 2018;170:379-387.

[35] Schlaich J, Mayr G. Naturzugkuhltunne mit vorgespanntern Membranmantel. Bauingenieur 1974; 49:41-45,.

[36] Haaf W, Friedrich G, Mayr G, Schlaich J. Solar chimneys, part I: principle and construction of the pilot plant in Manzanares. International Journal of Solar Energy 1983, 2: 3-20.

[37] Haaf W. Solar chimneys, part II: preliminary test results from the Manzanares pilot plant. International Journal of Solar Energy 1984, 2: 141-161.

[38] Menter FR. Two-Equation Eddy-Viscosity Turbulence Models for Engineering Applications. AIAA Journal 1994, 32: 1598-1605.

[39] Ming T. Solar Chimney Power Plant Generating Technology. Academic Press, Elsevier Inc.; 2016.

[40] Gannon A. J von Backström TW. Solar chimney cycle analysis with system loss and solar collector performance. Journal of Solar Energy Transactions ASME 2000;122:133-137.

[41] Pretorius JP, Kröger DG. Solar chimney power plant performance. Journal of Solar Energy Transactions ASME 2006;128:302-311.

[42] Nizetic S, Ninic N, Klarin B. Analysis and feasibility of implementing solar chimney power plants in the Mediterranean region. Energy 2008;33:1680-1690.

Highlights

- A novel solar chimney tower concept is proposed.
- The new concept enhances the system performance.
- Power output improvement reaches 32%.
- Outflow control method reduces tower costs by 40% for power reduction of only 6%.

Credit Author Statement

Title of the article:

"*Numerical investigation of a novel tower solar chimney concept*"

We, the undersigned, authors of this article**,** declare that this manuscript is original, has not been published before and is not currently being considered for publication elsewhere.
We confirm that the manuscript has been read and approved by all named authors and that there are no other persons who satisfied the criteria for authorship but are not listed. We further confirm that the order of authors listed in the manuscript has been approved by all of us. The contribution of each author is as follows:

Hakim Kebabsa: Conceptualization, Methodology, Software, Validation, Writing- Original draft preparation **Mohand Said Lounici**: Conceptualization, Methodology, Supervision, Writing- Reviewing and Editing. **Ahmed Daimallah:** Writing- Reviewing and Editing,

Signed by all authors as follows:

Corresponding author Name: LOUNICI Surname: Mohand Said

Signature: Date: July 24, 2020

Author Name: KEBABSA Surname: Hakim

Signature: Date: July 24, 2020

Author Name: DAIMALLAH Surname: Ahmed

Signature: Date: July 24, 2020

Declaration of interests

Title of the article:

"Numerical investigation of a novel tower solar chimney concept"

As the authors of this article we declare:

☐ The authors declare that they have no known competing financial interests or personal relationships that could have appeared to influence the work reported in this paper.

☐The authors declare the following financial interests/personal relationships which may be considered as potential competing interests:

Corresponding author Name: LOUNICI Surname: Mohand Said

Signature:  Date: April 1, 2020

Author Name: KEBABSA Surname: Hakim

Signature:  Date: April 1, 2020

Author Name: DAIMALLAH Surname: Ahmed

Signature:  Date: April 1, 2020